The snowflake divertor

D. D. Ryutov and V. A. Soukhanovskii

Citation: Physics of Plasmas **22**, 110901 (2015); doi: 10.1063/1.4935115
View online: http://dx.doi.org/10.1063/1.4935115
View Table of Contents: http://scitation.aip.org/content/aip/journal/pop/22/11?ver=pdfcov
Published by the AIP Publishing

The snowflake divertor

D. D. Ryutov and V. A. Soukhanovskii
Lawrence Livermore National Laboratory, Livermore, California 94550, USA

(Received 28 April 2015; accepted 19 October 2015; published online 17 November 2015)

The snowflake magnetic configuration is characterized by the presence of two closely spaced poloidal field nulls that create a characteristic hexagonal (reminiscent of a snowflake) separatrix structure. The magnetic field properties and the plasma behaviour in the snowflake are determined by the simultaneous action of both nulls, this generating a lot of interesting physics, as well as providing a chance for improving divertor performance. Among potential beneficial effects of this geometry are: increased volume of a low poloidal field around the null, increased connection length, and the heat flux sharing between multiple divertor channels. The authors summarise experimental results obtained with the snowflake configuration on several tokamaks. Wherever possible, relation to the existing theoretical models is described. © *2015 AIP Publishing LLC*.
[http://dx.doi.org/10.1063/1.4935115]

TABLE OF CONTENTS

LIST OF ACRONYMS

ADX	Advanced divertor experiment
ASDEX	Axially symmetric divertor experiment
CFETR	China's Fusion Engineering Test Reactor
CHI	Coaxial helicity injection
CREST	Conceptual reactor study
DIII-D	Doublet III-D
EAST	Experimental advanced superconducting tokamak
ECH	Electron cyclotron heating
EFIT	Equilibrium and reconstruction FITting code
ELM	Edge-localised mode
FAST	Fusion advanced studies torus
ITER	International thermonuclear experimental reactor
MARFE	Multifaceted asymmetric radiation from the edge
MAST	Mega ampere spherical tokamak
MHD	Magneto-hydro-dynamics
NSTX	National spherical torus experiment
PDX	Poloidal divertor experiment
PF	Poloidal field
RMP	Resonant magnetic perurbations
SF	Snowflake
SOL	Scrape-off layer
SOLPS	Scrape-off layer plasma simulator code
SP	Strike point
TCV	Tokamak à configuration variable
TF	Toroidal field
UEDGE	Universal EDGE code

I. INTRODUCTION

In the future tokamak-based fusion reactors, the generated thermal power will be in the range of 1–2 GW.[1]

Approximately 80% of it will be released in the form of 14 MeV neutrons, will leave the plasma across the magnetic field, go through the walls of the confinement vessel, and be absorbed in the tritium-breeding blanket. The other 20% of the power will be released in the form of the 3.5 MeV alpha-particles and transferred directly to the fusing plasma. In the steady-state mode, this power is balanced by the electron and ion heat transport to the boundary of the confinement zone and radiative loss from the confinement region. The latter is almost isotropic and spreads the radiated power evenly over the surface of the vacuum vessel. This channel of the energy loss has to be modest-to-small, as otherwise a volumetric cooling would lead to lower temperatures in the plasma core and reduce the power generation.[1–5] So, a substantial fraction of the power will be crossing the plasma boundary in the form of the electron and ion heat flux. Added to the fusion power should be the power delivered by the plasma control systems (such as the current drive). This would lead to the electron and ion flux through the plasma boundary in the range of ~200 MW.[1]

The burning plasma is not a perfectly controlled, static object: it is more like a burning flame, continuously flickering, with occasional tongues of flame darting from its surface and leading to bursts of heat flux in a hard-to-predict areas of the vessel. The problem is aggravated by that the vessel is not smooth, with a number of ports, diagnostic units, antennas, etc., making it quite "rugged." So, if "left alone," the plasma will soon "burn a hole" in the vacuum vessel.

All this was clear from the early days of fusion research and, in order to avoid uncontrolled damage to the elements of the inner surface of the confinement vessel, Spitzer[6] has proposed a special configuration of the magnetic field, with a magnetic field null on a certain flux surface that would create a singular flux surface ("the separatrix") beyond which the field lines would be open. The electron and ion heat flux would then be "diverted" from the walls and rapidly channelled along the field lines to the thermally and mechanically hardened surfaces of the "divertor."

A generic shape of the toroidally symmetric divertor configuration for tokamaks is shown in Fig. 1. A singular point where a self-intersection of the separatrix occurs is a null of the poloidal magnetic field. If, as it is typically assumed, the plasma current in the null area is small, the field in the vicinity of the null scales linearly with the distance r from the null and forms thereby a first-order null of the magnetic field (see more on that in Sec. II). The separatrix branches intersect at 90°.

Divertor experiments performed by the ASDEX group in Germany[7] have revealed that, in addition to diverting the plasma flux from the walls, the divertor may also have a significant favourable effect on the plasma parameters *inside* the separatrix, as manifested by the transition to a so-called High-confinement mode, or H-mode. This mode is characterized by a formation of a layer with steep density and temperature rise (from <100 eV at the separatrix to 1–2 keV a few millimetres inward) that creates a "pedestal" for the core density and temperature distributions and thereby significantly improves performance of the core plasma. Although the H-mode was later found in a variety of fusion devices

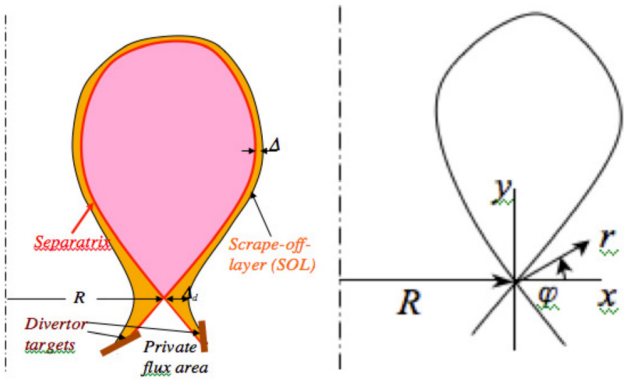

FIG. 1. Poloidal divertor notation and divertor coordinates: (a) The core plasma is shown in pink, the separatrix in red, and the SOL in orange. The SOL thickness at the midplane is denoted by Δ, whereas the SOL thickness near the divertor null, by Δ_d. The divertor plates (called sometimes "targets") are shown in brown; the intersection points of the separatrix with the plates are called "strike points," and an area where the SOL intersects the plates is called a "wetted area." An area below the null is called the private flux area. The field lines in this area do not enclose the core plasma, whereas the field lines in the SOL, do. The plasma density gradually decreases across the SOL in the direction away from the separatrix; the outer boundary shown in the figure is actually smooth. Some amount of plasma may also penetrate into the private flux region. (b) The divertor coordinates: The dash-dotted line is a tokamak geometrical axis; R is a radial distance between the axis and the PF null. Configuration shown corresponds to a single-null standard divertor. If similar configuration is created near the top of the confinement area, one obtains a double-null standard divertor.

not necessarily using a poloidal divertor (see a review of Ref. 8), the interaction of the pedestal and divertor remains an important issue in the physics of edge plasma and power exhaust for the existing and future tokamaks. Certainly the divertor and core are in a constant and significant interaction (e.g., via the plasma fuelling, MARFE formation, modifications of the ELM activity, and neoclassical orbits in the pedestal/SOL areas, as discussed later in this tutorial) and analysis of the heat exhaust problem requires accounting for the interaction between the plasmas on open and closed field lines.

Having greatly improved prospects for an acceptable survivability of the vacuum vessel, the divertor created a new problem: in practical designs, the heat flux on the surface of the divertor plates (Fig. 1(a)) turns out to be quite high. It depends obviously on the width of the scrape-off layer as projected on the divertor plates.

Making some assumptions about the geometry of the divertor region, one can roughly evaluate this flux. This has been done for divertor configurations of the type shown in Fig. 1(a) and has led to a prediction[1,2] that the heat fluxes can be as high as 60 MW/m^2 in the "regular" mode of operation and even higher in the bursts in the heat flux during so-called ELM events (see Sec. IV B). To appreciate the magnitude of the problem, one can mention that similar heat fluxes are present on the surface of the Sun and on the sacrificial nose-cone of the Space Shuttle during its re-entry (in the latter case, though, for less than 1 min). A summary of the heat loads in various facilities is presented in Table 1 of Ref. 9. An acceptable level for future reactors is thought to be ~5 MW/m^2.[9]

Recent reviews of the divertor research (Refs. 9 and 10) can be recommended to the readers. Systematic discussion of the divertor physics can be found in Stangeby's book.[11] The book contains, in particular, description of the so called two-point divertor model that relates the SOL parameters in the upstream SOL and on the divertor plate, as well as further references. In order to put the snowflake divertor concept in the context of other approaches to the divertor problem, we briefly describe these other approaches in the next few paragraphs. Those are by no means exhaustive and cannot serve as a substitute for the aforementioned reviews.

One of the approaches is based on the use of lithium as a coating for the divertor plates and, possibly, the walls of the vessel. One could also push lithium through the porous plates. Lithium may favourably change recycling coefficient for the hydrogen isotopes and its presence may significantly affect the particle and energy fluxes at the plasma boundary and, perhaps, improve the core plasma confinement as well, see Refs. 12–15. Lithium may also create a sacrificial, continuously renewable surface. Lithium vapour shielding is yet another potentially favourable effect.[12]

The other solution is a combination of seeding impurities to the divertor in order to increase radiation in the divertor zone and, at the same time, preventing them from penetration to the upstream SOL by enhancing the hydrogen plasma flow to the divertor. This can, in particular, be made in a double-null configuration with deuterium puffing in the upper divertor. As the radiation power flux is isotropic (does not follow the magnetic field lines), the heat-absorbing area becomes much greater than just the plasma-wetted area, if the power radiated on the way of the plasma to the divertor target is large.[16–18]

One may attempt to increase the SOL width by exciting toroidally asymmetric convection in the SOL, either by active manipulation of the potential of the divertor tiles or by making tiles wavy, or by using non-axisymmetric gas puffs.[19–21]

An additional element that is desirable (and, perhaps, even necessary) to make divertor workable in the fusion reactor environment is an effect called "detachment." In its full, somewhat idealized form, this is a formation of the recombination front in the divertor leg, so that in the vicinity of the divertor plate the plasma becomes weakly ionized and relatively cold;[3,4,22,23] the plasma loses its momentum via collisions with the recycling neutrals. Detachment reduces erosion of the divertor plates that can be significant if the plate is subjected to the flow of ionized particles. The recombination is accompanied with isotropic radiation, and the heat absorbing area increases compared to the plasma-wetted zone. Detachment is facilitated by reducing the heat flux to the target, so that the poloidal magnetic flux expansion in the divertor area is an important factor in the onset of detachment.

One can use double-null divertors, where the poloidal field null shown in Fig. 1 is created also at the top part of the separatrix, thereby splitting the heat flux between the upper and lower targets (see, e.g., Sec. 3 in Ref. 24). There are also subtler effects associated with separating connection between the inboard and outboard SOL and affecting stability properties of the SOL plasma. One can go even further and create a third null, near the equatorial plane, as described in a conceptual paper by Kesner,[25] or even four nulls, as realized in the PDX facility.[26]

A widely used technique for the heat flux reduction is tilting the divertor plates with respect to the poloidal field. This leads to increase of the wetted area and heat flux reduction. This technique is compatible with most of the divertor concepts, if the divertor legs are sufficiently long. One of the constraints on the allowable tilt is the requirement that the intersection angle of the total (toroidal plus poloidal) magnetic field vector should not be too shallow, to avoid formation of hot spots that may appear, in particular, due to the fact that the divertor floor is made of discrete tiles.

During the last 10–15 years, there appeared several further suggestions related to modification of the poloidal magnetic field structure. One of them suggested by Takase[27] is based on the flaring of the poloidal field lines in the vicinity of the strike points by using additional sets of coils that would create a magnetic field directed oppositely to the one of the initial configuration of Fig. 1. This generates "cusp" configurations where additional PF nulls are formed in the vicinity of the strike points. A similar approach has been described by Kotschenreuther *et al.* in Refs. 28, 29, and 5 and called an X-divertor. A clear verbal description of the concept was presented in Ref. 5: "This extra downstream X-point can be created with an extra pair of poloidal coils… Each divertor leg (inside and outside) needs such a pair of coils… The distant main plasma is hardly affected because the line flaring happens only near the extra coils." An elegant suggestion of bringing the divertor coils as close as possible to the null points by inserting small segmented coils in the gaps between the toroidal field coils was made in Refs. 28 and 29 (see, in particular, Fig. 1 in Ref. 28 and Fig. 5 in Ref. 29 for the coil system for the CREST reactor study).

One can produce strong flux expansion not in both, but in a single divertor leg. This has actually been done experimentally in 2001 by Pitts *et al.* on the TCV facility,

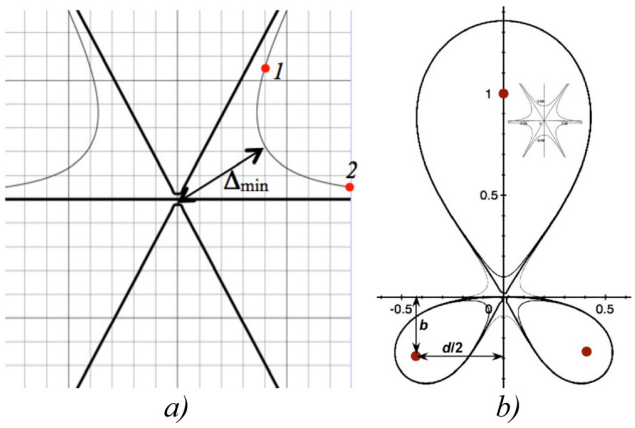

FIG. 2. An exact snowflake configuration: (a) Hexagonal separatrix and nearby flux surfaces; (b) a global structure of the magnetic field for the three-wire model of Ref. 34; the distances in (b) are normalized to the distance of the wire imitating the plasma current from the origin. Reprinted with permission from Phys. Plasmas **14**, 064502 (2007). Copyright 2007 AIP Publishing LLC.

where "varying degrees of detachment are obtained depending on the magnitude of the imposed outer divertor flux expansion," Ref. 30 (see Fig. 1 in that paper). The authors have not proposed a name for this interesting configuration.

Another approach is based on the coil arrangement that would allow one to pull the outer divertor leg in the outward direction so that the major radius of the strike point would be as large as compatible with the size of the toroidal coils.[31] This approach is known under the name of a "super-X divertor"[31] and will be tested on the upgraded version of the MAST tokamak where the poloidal field coils were designed in a way that would allow the generation of the super-X configuration.[32,33]

The use of the divertor coils situated near the strike points certainly provides a significant flexibility in controlling the shape of the flux surfaces in this zone. On the other hand, putting them there creates significant technological problems, especially in the reactor environment.

References 34–36 opened a series of analyses directed towards understanding of the degree of control of the magnetic field structure in the divertor region by the set of remote coils, situated, desirably, outside the TF coils. It turned out that, indeed, the remote coils allow creation of a broad variety of PF configurations of interest for the divertor design. In particular, it turned out to be possible to create a second-order null of the poloidal field, i.e., the configuration where the magnetic field would scale as r^2 with the distance r from the null. This, obviously, leads to formation of a large area of a weak poloidal field in this zone. The separatrix in the case of a second-order null acquires a characteristic hexagonal structure Fig. 2. This prompted the designation of the corresponding configurations as "snowflakes." As was explained in the first snowflake publication,[34] the exact second-order null is topologically unstable and splits into two nearby first-order nulls, maintaining, however, the general property of significant flux expansion. Two significantly different ways of how these nulls may split were identified and the terms "snowflake-plus" and "snowflake-minus" were introduced to designate the ensuing configurations. In that paper, only symmetric with respect to the vertical plane configurations were considered. In Ref. 35, a much more detailed analysis of the SF+ configuration was presented; the way for analysing asymmetric SF configurations was described. In Ref. 36, all the magnetic configurations with two nearby nulls have been identified, both symmetric and asymmetric. Relation of the flux surfaces and the properties of the global magnetic field have been established.

These three papers provide a framework for the discussion of the snowflake properties in our tutorial, see, in particular, Secs. II and III. An important feature of this discussion is the notion that these two nulls act in concert and are "communicating" to each other in a significant way.

The characteristic multi-sector structure of the magnetic field in the null-points of the first, second, and higher order is a direct property of the Laplace equation. Such structures have been used in the fusion research for stabilizing the mirror devices ("Ioffe bars"[37]) as well as in confinement systems for toroidal plasmas (toroidal multipoles), where the first, the second, or higher-order null was situated near the center of the poloidal cross-section (see, e.g., Refs. 38–40). The second-order null could also be transitionally formed inside the plasma in the course of plasma formation.[41] We are, however, not aware of the discussion and/or use of these field structures as magnetic divertors prior to Ref. 34.

During the last few years, the snowflake configurations has been produced and studied on several tokamaks, was a subject of numerous theory analyses, and has even entered the realm of reactor design studies. Their promises as well as their problems have been studied in significant detail. It is therefore timely to summarize the basic features of the SF divertors as understood now and relate them both to experimental results and possible reactor applications.

This tutorial is organized as follows. In Sec. II, we discuss geometrical features of the poloidal magnetic field for the snowflake divertor, with a focus on the idealized, "exact" snowflake. Sec. III is devoted to analysis of the two-null representation for the near-snowflake magnetic structures and their experimental realization and configuration control. In Sec. IV, we consider effect of the two-null geometry on the scrape-off layer and heat-flux sharing between multiple divertor legs, presenting experimental results from several tokamaks. Section V contains discussion of the effects that may be responsible for the heat-flux sharing. Sec. VI describes prompt ion losses from the snowflake divertor—a process that may affect the pedestal physics. The experimental results on the changes of core and pedestal behaviour between the standard and snowflake cases are presented in Sec. VII. Sec. VIII is focused on the experiments on radiative divertors and plasma detachment. Sec. IX discusses various versions of the snowflake divertors for future fusion reactor. Sec. X contains an outlook and a brief summary. Several more lengthy calculations are placed in Appendixes.

When describing the status of the theoretical understanding of the snowflake, we identify unsolved theory problems and challenge the theorists to solve them. We provide some brief explanation for why a particular problem may be important. We also identify and highlight situations where there is a lack of experimental information, or the present theory does not match experimental results.

II. THE MAGNETIC FIELD STRUCTURE FOR THE FIRST- AND SECOND-ORDER POLOIDAL FIELD NULLS

A. The poloidal field structure near the null

In the vicinity of the poloidal field null, for the distances significantly less than the major radius, the structure of the poloidal field can be well represented by a planar approximation, with the vector $\boldsymbol{B_p}$ having two components $B_x(x,y)$ and $B_y(x,y)$, with the local coordinate frame (x,y) shown in Fig. 1. For a planar field, the condition $\nabla \cdot \boldsymbol{B} = 0$ reads as

$$\frac{\partial B_x}{\partial x} + \frac{\partial B_y}{\partial y} = 0. \tag{1}$$

This equation generates a flux function $\Phi(x,y)$ such that

$$B_x = -\partial\Phi/\partial y; \quad B_y = \partial\Phi/\partial x. \tag{2}$$

The condition $\Phi(x,y) = \text{const}$ describes poloidal flux surfaces. The poloidal magnetic flux between two flux surfaces is constant. The function Φ as introduced by Eq. (2) has a meaning of the poloidal flux per unit length in the toroidal direction. Corrections to this model caused by the toroidicity effects (the finite value of the toroidal curvature) are discussed in Appendix A.

If one neglects the presence of the toroidal current in the area of the null (the plasma here is cold and has low density), one can state that the field is curl-free, i.e.,

$$\frac{\partial B_y}{\partial x} - \frac{\partial B_x}{\partial y} = 0. \tag{3}$$

This equation then generates a scalar potential Ψ,

$$B_x = -\partial\Psi/\partial x; \quad B_y = -\partial\Psi/\partial y. \tag{4}$$

Substituting Eq. (2) into Eq. (3), one finds that the flux function satisfies Laplace equation,

$$\frac{\partial^2\Phi}{\partial x^2} + \frac{\partial^2\Phi}{\partial y^2} = 0 \tag{5}$$

(the same is true for the scalar potential).

The planar curl-free magnetic field can be conveniently described by the machinery of the complex variables,[42] with the complex position being

$$z = x + iy, \tag{6}$$

and the field being a complex function $F(z)$ defined by:

$$\text{Re}F = B_x; \quad \text{Im}F = -B_y. \tag{7}$$

We call F "a field function." The absolute value of the field is $|F|$.

Equations (1) and (3) constitute the Cauchy-Riemann conditions for the complex function F, which is, therefore, a regular function. The complex flux function $G(z) = \Psi + i\Phi$ is regular by virtue of Eqs. (2) and (4) and is related to the field function via $F = -dG/dz$, so that

$$B_x = -\text{Re}(dG/dz), B_y = \text{Im}(dG/dz). \tag{8}$$

We are interested in the systems where PF coils are situated far away from the divertor nulls and, therefore, the flux-function around the nulls is a smooth function of the coordinates. Near the simple (first-order) null, the magnetic field is a linear function of coordinates

$$F = A_1 z, \tag{9}$$

where A_1 is a constant multiplier (generally speaking, complex). The subscript "1" refers to the first-order null. Absolute value of A_1 determines the gradient of the field strength near the null. In the midplane SOL, i.e., at the distance of order of a minor radius a from the divertor null, the poloidal field reaches a value of B_{pm}, where the additional subscript "m" refers to the midplane. So, the natural measure for the field gradient is $|A_1| \sim B_{pm}/a$. We will introduce also a dimensionless form-factor $K_1 \sim 1$ that may vary from one global configuration to another. In other words, we represent A_1 as

$$A_1 = K_1(B_{pm}/a)e^{i\eta}. \tag{10}$$

The parameter η characterizes the orientation of the separatrix branches with respect to the geometrical axis.

The complex potential is, obviously,

$$G = -A_1 z^2/2 = -K_1(B_{pm}/a)e^{i\eta}z^2/2, \tag{11}$$

where we set an arbitrary additive constant to zero. The equation $\text{Im}G = 0$ describes then a flux surface passing through the null, i.e., the separatrix. Other flux surfaces are described by $\text{Im}G = \text{const}$, where the r.h.s. specifies the flux Φ between the separatix and this flux surface (we remind that Φ is a flux per unit length in the toroidal direction).

Fig. 3(a) shows the shape of the separatrix and a nearby flux surface for $\eta = \pi/2$, whereas Fig. 3(b) corresponds to $\eta = -\pi/3$. In order to compare the flux surface *shapes* and not be confused by the overall tilts characterized by the parameter η, in the further discussion, we will always choose the orientation, where the bisector of the separatrix branches is strictly vertical (parallel to the geometrical axis). By replacing z by $z - z_0$, one could shift the null from the origin, but further on we will always place the origin to the field null lying on the main separatrix, thereby setting $z_0 = 0$.

The absolute value of the magnetic field, $|\boldsymbol{B}_p| = \sqrt{B_{px}^2 + B_{py}^2}$, is $|dG/dz| = |A_1||z|$, or

$$|\boldsymbol{B}_p| = K_1 B_{pm} r/a, \tag{12}$$

so that the absolute value of the magnetic field does not depend on the polar angle φ (Fig. 1(b)) and scales linearly with the distance from the null. The right-hand side of the equation $dB_p/dr = K_1 B_{pm}/a$ determines the radial derivative of the polodal field at the null. If written in the form

$$\frac{(B_{pm}/a)}{(dB_p/dr)} = \frac{1}{K_1} \equiv \kappa, \tag{13}$$

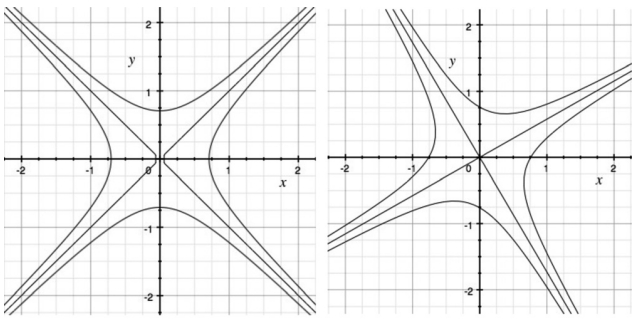

FIG. 3. Parameter η and orientations of the separatrix for the first-order null: (a) $\eta = \pi/2$ and (b) $\eta = -\pi/3$.

it yields a quantity $\kappa \equiv 1/K_1$ that we will call a "flatness" of the divertor field: the larger this coefficient, the "flatter" the field is, with a larger zone around the null where the field is weak. When the divertor coils are situated at the distances exceeding the minor radius, this coefficient K_1 is of the order one. One can deliberately make K_1 large by placing the divertor coils very near the null, as it was done, in particular, in the old ASDEX divertor.[43] The flatness then is low, and the poloidal field near the null grows steeply.

Consider now the situation where we have two nearby field nulls, with one of them lying on the main separatrix, i.e., for our choice of the origin, at $z=0$. One would then have for the function F,

$$F = A_2 z(z - z_2), \tag{14}$$

where z_2 is the second null (with the first null situated at the origin), and

$$A_2 = K_2 B_{pm} e^{i\eta}/a^2. \tag{15}$$

with $K_2 \sim 1$. Integrating F, one finds the complex potential

$$G = -A_2\left(\frac{z^3}{3} - \frac{z_2 z^2}{2}\right), \tag{16}$$

where the arbitrary additive constant is set to zero, so that $\mathrm{Im}G = 0$ corresponds to the main separatrix. To find the second separatrix, the one that passes through $z = z_2$, one has to solve an equation $ImG(z) = ImG(z_2)$

$$\mathrm{Im}\left[e^{i\eta}\left(\frac{z^3}{3} - \frac{z_2 z^2}{2}\right)\right] = -\mathrm{Im}\left[e^{i\eta}\frac{z_2^3}{6}\right]. \tag{17}$$

The orientation of the asymptotes of the main separatrix is determined by the parameter η; we will further set it equal to zero, so that the separatrix will be oriented as shown in Fig. 2(a). The confinement zone will then occupy the upper central sector of the xy plane.

B. The poloidal field characterization for an "exact" snowflake

We start from considering the situation where the two nulls coincide ($z_2 = 0$) and form thereby a single second-order null. In Secs. III and IV, we will expand the analysis to a more general and practically more important case of a finite z_2. According to Eqs. (14) and (15), the magnetic field behaves then as

$$F = K_2(B_{pm}/a^2)z^2, \tag{18}$$

where we have set $\eta = 0$ per our convention regarding the identification of the confinement zone. An absolute value of the magnetic field strength is

$$B_p = |F| = K_2(B_{pm}/a^2)r^2. \tag{19}$$

It depends only on the distance r to the second-order null. The change of the dependence from the linear (as in the standard X-point case) to quadratic has strong effect on the poloidal magnetic field. In particular, the poloidal field magnetic pressure scales as r^4 and is very small in the vicinity of the second-order null (for example, for $r = 0.2a$ and $K_2 \sim 1$, the poloidal field pressure is $\sim 10^{-3}$ of its value at the mid-plane). This simple observation may be significant when assessing the plasma behaviour near the null.

We tag each flux surface with its minimum distance from the null Δ_{min} (Fig. 2). For a given Δ_{min}, one can evaluate the poloidal magnetic flux between the separatrix and this flux surface, $\Phi(\Delta_{\min})$. Obviously, for the dependence (19), this flux is

$$\Phi(\Delta_{\min}) = K_2(B_{pm}/3a^2)\Delta_{\min}^2. \tag{20}$$

Now, we recall that in the toroidal system the poloidal flux $\tilde{\Phi}$ over the whole toroidal circumference is related to Φ by: $\tilde{\Phi}(\Delta_{\min}) = 2\pi R_0 \Phi(\Delta_{\min})$, where R_0 is a radius of the line formed by the PF nulls (a circle surrounding the geometrical axis). Here, we assume that the thickness Δ of the poloidal annulus is small compared to R_0. Consider the same flux surface near the mid-plane. We denote its distance from the separatrix at the mid-plane as Δ. The poloidal magnetic field in the vicinity of the separatrix near the mid-plane is almost uniform over the SOL thickness, so that

$$\tilde{\Phi}(\Delta) = 2\pi R_m B_{pm}\Delta, \tag{21}$$

where R_m is the plasma major radius at the midplane (for definiteness, we consider the outboard radius). Equating $\tilde{\Phi}(\Delta)$ and $\tilde{\Phi}(\Delta_{min})$, we find that

$$\frac{\Delta_{\min}}{a} = \left(\frac{3R_m}{R_0 K_2}\right)^{1/3}\left(\frac{\Delta}{a}\right)^{1/3}, \tag{22}$$

or, equivalently,

$$\frac{\Delta_{\min}}{\Delta} = \left(\frac{3R_m}{R_0 K_2}\right)^{1/3}\left(\frac{a}{\Delta}\right)^{2/3}. \tag{23}$$

The first factor in Eq. (23) is of order one, whereas the second one is very large and depends on the distance from the separatrix. The closer to the separatrix, the stronger effect. Equations (22) and (23) are equally valid *inside* the separatrix.

Taking as Δ the mid-plane SOL thickness identified with the widely used parameter λ_q (the width of the heat flux on the target projected along the flux surfaces to the mid-plane), one finds that for the ITER-like tokamak, with $a \sim 250$ cm and $\lambda_q \sim 0.3$ cm, one could expect very strong flaring of the poloidal flux near the second-order null, $\Delta_{\min}/\lambda_q \sim 90$.

For comparison, we present similar results for a standard X-point divertor described by Eqs. (9) and (10)

$$\frac{\Delta_{\min}}{a} = \left(\frac{2R_m}{R_0 K_1}\right)^{1/2}\left(\frac{\Delta}{a}\right)^{1/2}; \quad \frac{\Delta_{\min}}{\Delta} = \left(\frac{2R_m}{R_0 K_1}\right)^{1/3}\left(\frac{a}{\Delta}\right)^{1/2}. \tag{24}$$

For the just considered numerical example ($a \sim 250$ cm and $\Delta \sim 0.3$ cm), one would have for the standard divertor 3 times weaker flux expansion, $\Delta_{\min}/\lambda_q \sim 30$.

Likewise, if one considers the poloidal field strength at the *same* modest distance r from the null ($r/a < 0.3-0.4$),

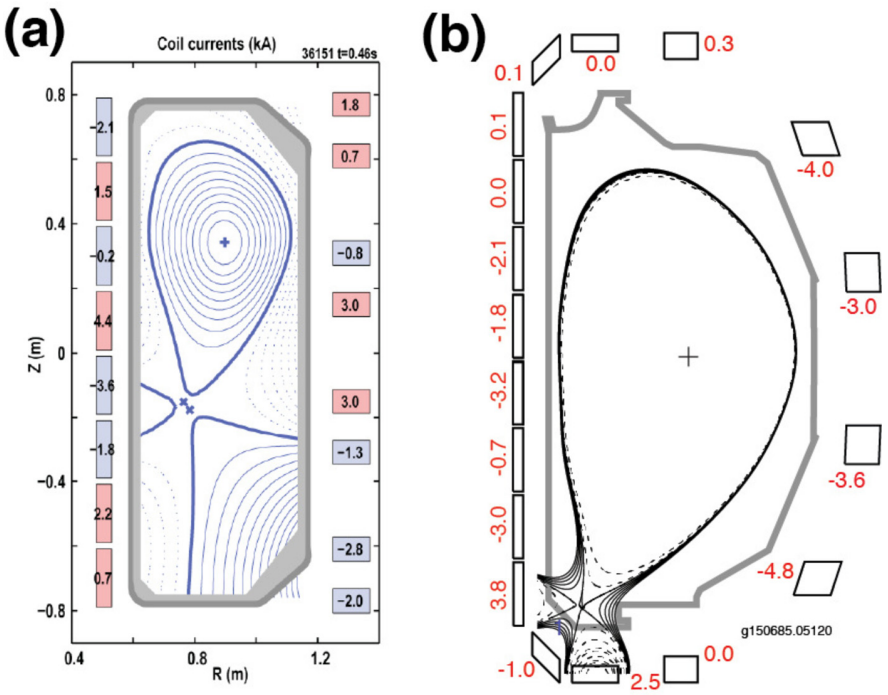

FIG. 4. Plasma equilibria with the snowflake divertor configurations in the TCV (a) and DIII-D (b) tokamaks. The numbers next to the poloidal magnetic field coils indicate coil currents in kA. Note that both structures are tilted with respect to the vertical axis, i.e., the parameter η in Eq. (15) is different from zero. The difference in the tilt may be responsible for subtle differences of the divertor behaviour, see, in particular, Sections V C, V D, and VI below. Reprinted with permission from Soukhanovskii *et al.*, J. Nucl. Mater. **438**, S96 (2013). Copyright 2013 Elsevier.[44]

one finds that the poloidal field at this distance is smaller for the snowflake, due to the quadratic vs. linear dependence of B_p on r. At a larger distance from the null, the dependence of B_p on r loses its universality (the power law) and the field structure becomes device-dependent.

Considering the flux surfaces just inside the separatrix and using Eqs. (23) and (24) with Δ measured in the inward direction, one sees that the distance of the pedestal inner "boundary" is much further from the snowflake null than from the standard null. This simple example shows that the effect of a snowflake on the processes *inside* the separatrix also can be significant.

These features of the snowflake configuration are seen in the equilibrium analyses for the configurations obtained on TCV and DIII-D in Fig. 4. Hexagonal separatrix structures and very large flux expansion near the null (as seen from the shape of nearby flux surfaces) are clearly visible.

For reference purpose, we provide here brief information on these facilities, as well as on the spherical torus NSTX, where a number of snowflake divertor experiments was performed.[45–47] TCV[45] is a device with a large number of poloidal field coils that allow for high degree of control over the plasma shapes; NSTX[46] is a spherical (low aspect ratio) tokamak, and DIII-D[47] is a large tokamak with high plasma current and high heating power. Table I summarizes typical parameters of these devices in the snowflake experiments. In this table, B_t is the toroidal field strength, I_p is the plasma current, P_{aux} is auxiliary heating power (NBI in NSTX and DIII-D, and ECH in TCV), R and a are the major and minor plasma radius, and λ_q is an e-folding length of the heat deposition as projected along the flux surfaces to the midplane. All three devices had graphite plasma-facing components and operated in L- or H-modes with auxiliary heating with BxgradB toward the lower (snowflake) divertor (in TCV, some shots related to the effects of particle drifts on the flux sharing between the multiple divertor legs[48] have been performed with a reversed toroidal field[49])

Now, we turn to more subtle features of the second-order null. The flux function for the exact snowflake ($z_2 = 0$ in Eq. (16)) is

$$\Phi = \mathrm{Im}G = \frac{K_2 B_{pm}}{3a^2}\left(y^3 - 3x^2 y\right). \tag{25}$$

Consider some field line whose minimum distance from the null is $\Delta_{\min}$ (Fig. 2). The position of the point closest to the null in the x,y coordinates is $x = \Delta_{\min}\sqrt{3}/2, y = \Delta_{\min}/2$, so that the equation that defines the field line passing at the minimum distance $\Delta_{\min}$ from the null reads as

$$y^3 - 3x^2 y = -\Delta_{\min}^3. \tag{26}$$

Take two symmetrical points, 1 and 2, whose distance from the null is $2\Delta_{\min}$, Fig. 2(a). We now evaluate the magnetic field line length L_{12} between these two points (so-called "connection length"). This length can be presented as an integral

TABLE I. Main engineering and plasma parameters of the tokamak snowflake experiments.

	B_t (T)	I_p (MA)	P_{aux} (MW)	R (m)	a (m)	λ_q (mm)
TCV	1.4	0.300	0–1.5	0.88	0.22	8
NSTX	0.5	0.8	4–6	0.85	0.65	6
DIII-D	2.0	1.2	1–5	1.70	0.60	2.5–3

$$L_{12} = \int_1^2 \frac{\sqrt{B_t^2 + B_p^2}}{B_p} dl \approx B_T \int_1^2 \frac{dl}{B_p}, \tag{27}$$

along the poloidal projection of the field line, with dl being a length element of this projection, and B_t being the toroidal field strength. When transitioning to the second equality in Eq. (27), we used the fact that $B_p \ll B_t$ and the toroidal field is nearly constant at small distances from the null (B_t scales as $1/R$). Expression (27) determines the contribution of the vicinity of the null to the total connection length L (target-to-target for the open field lines, and full 2π poloidal turn for the closed field lines). As we shall see, the contribution (27) becomes dominant for the field lines that are close to the separatrix.

Using Eq. (26) for the poloidal field line and Eq. (19) for the magnetic field, one finds the following expression for the field line length:

$$L_{12} \approx B_t \int_1^2 \frac{dl}{B_p} \approx 2.2 \frac{B_t}{K_2 B_{pm}} \frac{a^2}{\Delta_{\min}}. \tag{28}$$

The length of the segment of the field line traversing the zone of a weak poloidal field diverges for the flux surfaces approaching the separatrix, as the field line makes many turns in the toroidal direction before it leaves the null area. The divergence is a strong power-law divergence, $L \sim 1/\Delta_{\min}$. If one expresses L_{12} as a function of the distance Δ to the separatrix in the mid-plane, one finds that $L_{12} \propto 1/\Delta^{1/3}$ (see Eq. (22) relating Δ and $\Delta_{\min}$).

For the standard first-order-null divertor, the same calculation yields

$$L_{12} \approx 2.8 \frac{B_t a}{K_1 B_{pm}}. \tag{29}$$

As before, the points 1 and 2 are the points for which the distance to the null is two times higher than at the mid-point, i.e., $2\Delta_{\min}$. Eq. (29) indicates the absence of the power-law divergence for the standard null. The difference in the length of the flux tubes in the vicinity of the field null is directly related to the stronger poloidal flux expansion (weaker B_p) in the snowflake divertors.

In Eqs. (28) and (29), one could extend the integration from one divertor target to the other and find the total connection length, but this total length characterizes not so much the divertor region but rather the global plasma shape that is not much different between the standard and snowflake divertors. Still, we present here an expression for the target-to-target connection length L_{t-t},

$$L_{t-t} \approx \int_{t_1}^{t_2} \frac{B_t dl}{B_p}, \tag{30}$$

where the end-points are situated on the targets. Here, we do not take the B_t out of the integral. In the case of very small Δ, the target-to-target length diverges as $(a/\Delta)^{1/3}$ for the snowflake divertor and as $\ln(a/\Delta)$ for the standard divertor.

Consider two nearby flux surfaces confining the poloidal flux $\delta\tilde{\Phi}$. The volume δV of an annulus limited at the top and the bottom by the points 1 and 2 (Fig. 2(a)) or by divertor targets is

$$\delta V = \int_1^2 \frac{\delta\tilde{\Phi}}{|B_p|} d\ell = \delta\tilde{\Phi} \int_1^2 \frac{dl}{B_p}, \tag{31}$$

where the integration has the same meaning as in Eq. (28). An important parameter is specific volume $\delta V/\delta\tilde{\Phi}$ of this annulus. For tokamaks with a not too small aspect ratio, the toroidal field experiences only a modest variation between the midplane and the null. One can then assume that B_T is roughly constant along the integration path; also, one has $B_T \gg B_p$. With these observations made, and using Eq. (27), one finds that

$$\delta V_{12}/\delta\tilde{\Phi} \approx L_{12}/B_t, \tag{32}$$

so that the specific volume is proportional to L_{12} (cf. Eq. (5) in Ref. 50).

Therefore, according to Eqs. (29) and (32), the specific volume of flux annulus in the vicinity of the separatrix for the snowflake is much larger than for the standard divertor. The increased volume means that the radiation power from the low poloidal field zone will be higher for the snowflake (for the same plasma parameters), especially near the separatrix. This factor may have a favorable impact on divertor performance. Indications for this effect have indeed been found in numerical simulations (see below).

Switching now to the area of closed flux surfaces just inside the separatrix, one can evaluate the safety factor q defined in a standard way

$$q = \frac{1}{2\pi} \oint \frac{B_T dl}{R B_p}, \tag{33}$$

where the integration is carried out along a closed field line in the poloidal plane. If q is represented as a function of a distance Δ between the separatrix and a flux surface in a mid-plane, one would immediately find that for small Δ the q-factor diverges, logarithmically for the standard null, $q \propto \ln(a/\Delta)$, and as a power law, $q \propto (a/\Delta)^{1/3}$, for the snowflake. There will be also a strong divergence of the magnetic shear that is proportional to $dq/d\Delta$.

In the divertor physics, an important parameter is a so called flux expansion that can be introduced in the following way. Assume that at the mid-plane the *normal* distance between two flux surfaces is δ_m. The poloidal magnetic flux enclosed between these two flux surfaces is $2\pi R_m B_{pm} \delta_m$. Moving along the flux surface to the strike point, we can express the same flux as: $2\pi R B_p \delta$. We see that the ratio $\hat{f}_x$ of the *surface area* enclosed between the flux surfaces in these two positions (i.e., $(2\pi R\delta)/(2\pi R_m \delta_m)$) is simply

$$\hat{f}_x = \frac{B_{pm}}{B_p}. \tag{34}$$

The larger this parameter, the larger is the surface area of the "wetted" zone on the target, the stronger reduction of the heat flux one can anticipate. We emphasize that the poloidal

field flux enclosed by the annulus does not change, what changes is the surface area of the normal cross-section. If one is interested in the variation of the normal (to the flux surface) *width* δ, one finds

$$f_x = \frac{\delta}{\delta_m} = \frac{R_m B_{pm}}{R B_p}. \tag{35}$$

This parameter is also often called "flux expansion," alongside with $\hat{f}_x$.

If the plasma penetration to the private flux region of the main separatrix is small, as is usually the case in the standard divertor, these parameters are easy to use and interpret. The same relates to the situations with a snowflake divertor, if the plasma exhaust occurs mainly through the common flux region of the main separatrix.

However, in the case of a snowflake divertor, there is a possibility of "activation" of four strike points and corresponding heat flux sharing between all four of them (see Secs. IV and V). In this case, the use of the parameter (34) and (35) requires caution.

C. Summary of the plasma physics effects strongly influenced by the snowflake geometry

Before going to further discussion, we present here a summary of the effects that may be strongly influenced by the transition from the first to the second-order null. We will later include effects of a finite distance between the two nulls in the more general "approximate" snowflake cases. For the exact snowflake, these effects include:

1. Stronger flaring of the magnetic field and corresponding increase of the poloidal flux expansion (35) near the field null compared to the standard divertor: at the same (small) distance from the divertor null, the poloidal field of the SF divertor is lower than in the standard divertor. A significant additional effect comes from the related increase in the connection length. This leads to an increase of the temperature drop between the midplane and the target; a longer residence time of a certain parcel of plasma on its way to the target would also increase the radiative losses. Simulations of the SOL transport generally confirm these trends.[51–58] Transition to detached regimes is facilitated as observed experimentally (Sec. VII).
2. Change of the connection length and magnetic shear *inside* the separatrix, in the pedestal region, and possible effect on the pedestal transport and "germination" of ELMs. These are relatively subtle effects and the analyses performed so far show that the peeling-ballooning mode may be affected in a significant way,[59,60] whereas the other studies show that the effect may be weak.[61] A lot depends on details of the geometry—if the mode is sheared off before even reaching the vicinity of the null,[61] the localized changes of the field properties may become irrelevant; on the other hand, the modes with lower mode number may still be affected.
3. A counterpart of this effect on the open field lines, where a SOL intermittent transport (called also "blob" transport[62]) can be affected both by the increased blob length and a reduced connectivity to the target (reduced by a stronger shear, Ref. 63). In TCV, experiment significant reduction of the blob transport was observed (see Refs. 64 and 65; Fig. 14 below).
4. Effect on the neoclassical particle trajectories in the pedestal region. Those trapped ions whose turning points are situated near the second-order null spend there a very long time (as the connection length in this zone is very large) and experience large excursions with respect to the flux surfaces.[66] There is a dramatic increase of the prompt ion loss in the case of a "normal" orientation of the toroidal field, the one corresponding to the toroidal drift directed towards the null. This, in turn, may have an effect on the electric potential distribution in the pedestal area,[67,68] and thereby on the velocity shear.
5. Effect on the field stochastization near the second-order null caused by the presence of the zone of a very weak poloidal field. In particular, there may be an interesting change in the effect of the RMP coils.[69]
6. Possibe sharing of the heat flux between all divertor legs, occurring through a variety of potentially possible mechanisms: modified particle drifts,[48,49] flute-like and ballooning instabilities,[70] axisymmetric convection (a churning mode[71]), and magnetic field stochastization. This heat flux sharing is highly desirable as it would allow to fully realize the SF divertor potential in reducing heat flux and facilitating detachment in each of the strike points. If the flux sharing occurs via turbulent convection, it may also broaden the width of the wetted area in each of the divertor legs.[50,71]

Some of these effects have been observed experimentally (see below); some have not been clearly identified. The latter may be caused by the uncertainties in the theory predictions, or in the relative smallness of these effects. Some of them may be more important for the eventual solution of the divertor problem, the other may be less important. But, all of them can contribute to our better understanding of the divertor physics and, in their totality, make a snowflake divertor an excellent "divertor laboratory."[9,52]

III. SNOWFLAKE CONFIGURATIONS WITH TWO NEARBY NULLS

A. Classification of the ensuing field configurations

The realization of the fact that one has always to deal not with an exact second-order null, but with two nearby first-order nulls has been a part of the snowflake approach from the first publications[34,35] on this subject. A broad variety of ensuing configurations was assessed in Ref. 36. The characteristic geometries are illustrated by Fig. 5. One can characterize the position of the second null by its coordinates X_2 and Y_2, but a more convenient description was proposed in Ref. 36, where the position of the second null was characterized by its distance D from the first null and an angle ϑ between the x-axis and the direction to the null (Fig. 5(d)). It is assumed that this second null is situated in the lower half-space ($\vartheta > 0$ for the orientation shown in Fig. 5(d))

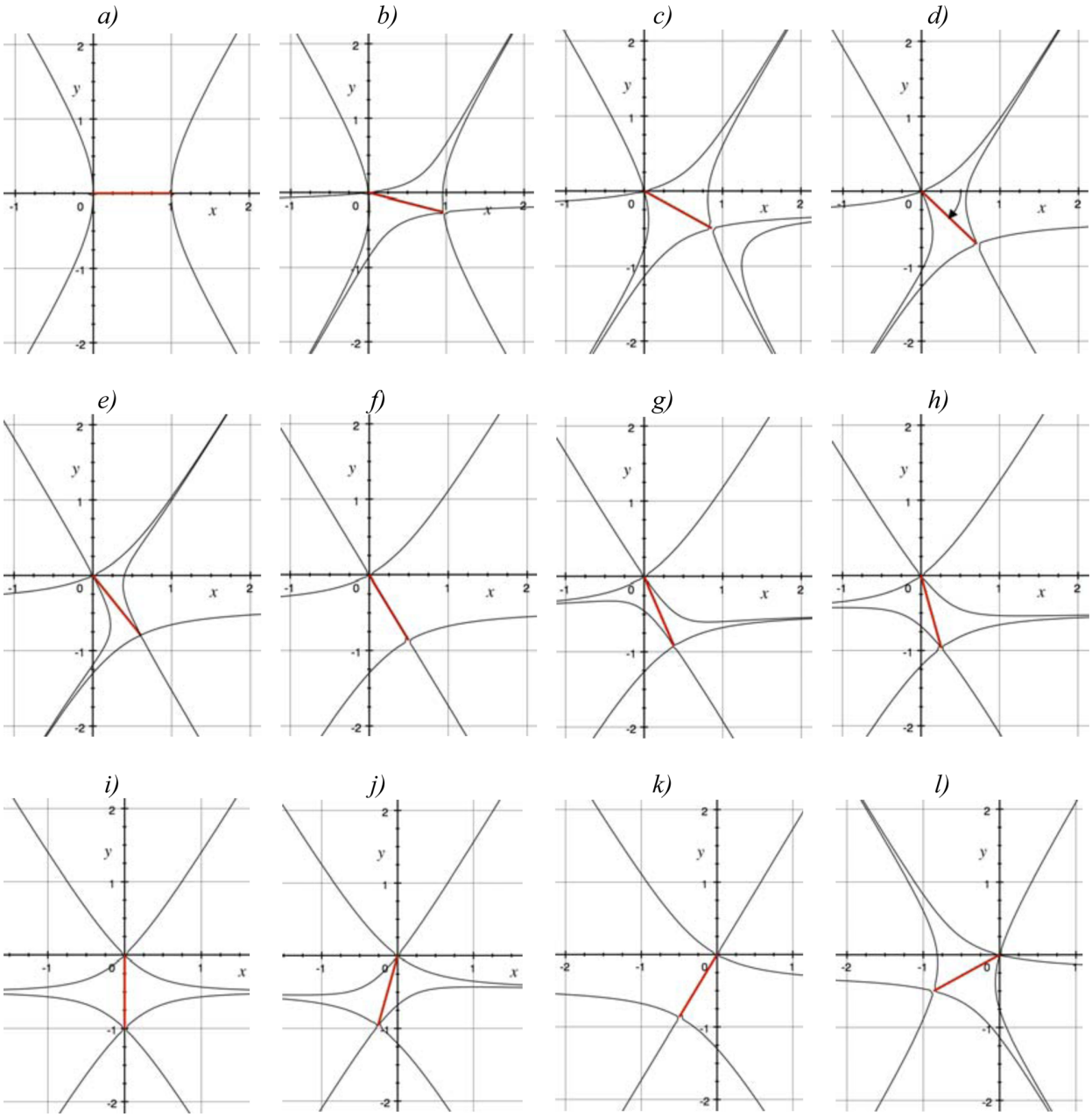

FIG. 5. Quasi-snowflake configurations. All the distances are normalized to the distance between the nulls, so that $D=1$ in all cases. Convention on the orientation is that $\eta=0$ (see Eq. (15)), so that the asymptotes to the upper branches of the separatrix form an angle $\pi/6$ with the y axis. Angle ϑ (shown in panel (d)) is measured between the right branch of the horizontal axis and red segment that connects two nulls. Cases for $\vartheta>\pi/2$ mirror the cases for $\vartheta<\pi/2$. Still, we have shown a few of them. Although they are mere reflections of the cases with $\vartheta<\pi/2$, they are not identical in a practical sense: if the tokamak geometrical axis is at the left, they may give rise to "activation" of different strike points, see discussion in Sec. IV A. Special cases (f) and (k) where both nulls lie on the same separatrix are topologically unstable. See further details in the text.

$$X_2 = D\cos\vartheta; \quad Y_2 = -D\sin\vartheta. \tag{36}$$

Normalizing all the distances to D and using equation $\mathrm{Im}G(z)=0$ for the primary separatrix and Eq. (17) for the secondary separatrix, with $\eta=0$ in both cases, one finds then the following single-parameter (ϑ) family of curves describing the primary and secondary separatrices:

$$-\frac{y^3}{3}+x^2y-xy\cos\vartheta+\frac{x^2-y^2}{2}\sin\vartheta=0, \tag{37}$$

$$-\frac{y^3}{3}+x^2y-xy\cos\vartheta+\frac{x^2-y^2}{2}\sin\vartheta=\frac{\sin 3\vartheta}{6}. \tag{38}$$

Several characteristic shapes are plotted in Fig. 5, starting from $\vartheta=0$ and moving on to higher ϑ. The configuration shown in Fig. 5(a) corresponds to $\vartheta=0$; both nulls are situated on the same separatrix. The split of the two nulls in the horizontal direction corresponds typically (albeit not universally) to a lower than "ideal" current in the divertor coils. This is why this configuration was called "snowflake-minus" in Ref. 34. This is in some sense an analogue of a

double-null divertor, but with the nulls situated not at the top and the bottom of the separatrix but close to each other near the bottom. As mentioned in Ref. 36, a condition that two nulls lie on the same separatrix makes this configuration topologically unstable to small perturbations of the coil currents (that determine, in particular, the angle ϑ): an infinitesimal change of ϑ eliminates connection between the two nulls along the flux surface. For example, for slightly increasing angle ϑ from zero to, say, $\vartheta = \pi/12$, we obtain a configuration shown in Fig. 5(b).

In this configuration, the secondary separatrix encloses the primary one, or, stated differently, the secondary null is situated in the common flux region of the main separatrix. Moving further, we see a sequence of these configurations maintaining the same topology until we reach the point where $\vartheta = \pi/3$, where we again find a situation where both nulls lie on the same separatrix. Configurations with $0 < \vartheta < \pi/3$ are formed as a gradual evolution of the initial SF− configuration of Fig. 5(a) and are all called "snowflake-minus" configurations. The configuration of Fig. 5(f) is again topologically unstable: it slips back into the snowflake-minus category if ϑ is slightly lower than $\pi/3$ (Fig. 5(e)) or joins a different, "snowflake-plus" category, for which the second null lies in the private flux region of the main separatrix (Figs. 5(g), 5(h), and 5(i)). The name "snowflake-plus" stems from the fact that it typically corresponds to a higher than "ideal" current in the divertor coils. Continuing to increase ϑ beyond $\pi/2$, we obtain "flipped" configurations. A few of these "flipped" configurations are shown in Figs. 5(j)–5(l).

As mentioned, the intermediate configuration of Fig. 5(f) is topologically unstable. If, however, one wants to use it in a practical divertor design, one can operate the PF coil system so that it would become one of the nearby topologically stable "plus" or "minus" configurations. An example of such configurations is illustrated by Figs. 5(e) and 5(g).

An important parameter of the two null configurations is the magnetic flux $\tilde{\Phi}_{12}$ enclosed between two separatrices. To find it, one notes that $\tilde{\Phi}_{12} = 2\pi R_0 \Phi_{12} = 2\pi R_0 \mathrm{Im} G(z_2)$ and uses Eqs. (15) and (16) with $\eta = 0$

$$\tilde{\Phi}_{12} = 2\pi K_2 R B_{pm} D^3 \frac{\sin 3\vartheta}{6a^2}. \tag{39}$$

This flux becomes zero when both nulls lie on the same separatrix. Within the segment $0 < \vartheta < \pi$, $\tilde{\Phi}_{12}$ turns zero for $\vartheta = \pi/3$ and $\vartheta = 2\pi/3$. Those are configurations shown in Figs. 5(f) and 5(k). They are both topologically unstable as, for an infinitesimal change of ϑ, they turn either to a snowflake-plus (like Fig. 5(g)) or snowflake-minus (like Fig. 5(e)), with a different connectivity of the sectors on the (x, y) plane.

Although the field structures shown in Fig. 5 look quite different from each other in the zone of the size $\sim D$, at larger distances they look as "exact" snowflakes. This is illustrated by Fig. 6 where two of the configurations of Fig. 5 are shown at lower "magnification" so that more distant part of the field structures becomes visible. One clearly sees that in this farther zone the six outgoing branches of the separatrix are essentially the same for both configurations. Figure 6 is discussed in more detail in Sec. III B. Here, we only mention that are using the following convention regarding the orientation of the separatrix: the confinement area lies in the upper sextant, with the y axis parallel to a bisector between asymptotes of the separatrix branches.

Another aspect of the characterization of the near-snowflakes is related to the issue of the reaction of the configuration to the possible imperfections in the adjustment of the PF currents. These issues have been discussed in the first snowflake publications[34,35] and are summarized in Appendix B. The conclusion is that the split D between the nulls scales as a square root of the current mismatch, which is often created deliberately, to operate in one of the topologically stable modes and/or study the physics associated with the finiteness of D.

Within the family of the near-snowflake structures of Fig. 5, there are snowflake-plus, snowflake minus, and intermediate configurations of Figs. 5(f) and 5(k) that are actually rotated configurations of Fig. 5(a). A smooth magnetic field (where the scale of the magnetic field variation is greater than null-to-null distance) in the zone of a negligible toroidal current *does necessarily look as one of the configurations shown in Fig. 5*, see Ref. 36. The underlying physics that determines this structure lies in very basic properties of the magnetic field (or, put it differently, of the Laplace equation). The existence of a simple analytical field representation is *a mere consequence of this physics* (certainly a fortunate consequence that allows one to easily uncover many interesting details). If the field is created by remote coils (situated at a distance sufficiently large compared to D), the field is automatically smooth. As mentioned in Sec. II, the remoteness is a desirable feature of a practical divertor.

As a common name for the configurations of Fig. 5, one can use a term "quasi-snowflakes" as was done in Refs. 54, 56, and 72. To designate a configuration intermediate between SF-plus and SF-minus, a special term "tripod" was

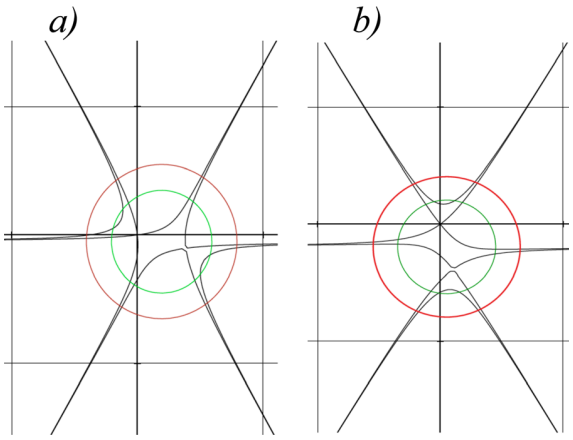

FIG. 6. The snowflake-minus (a) and snowflake-plus (b) configurations. Green circles show the zone, outside which the field becomes close to that of an exact snowflake. Red circles delineate a zone affected by the prompt loss or other snowflake-specific effect. If the size of the second zone is larger than that of the first zone, one can use the model of an "exact" snowflake to evaluate the effect in question.

introduced in Ref. 73, due to the three outgoing branches of the separatrix in the second null. Fig. 7 shows a geometry of one of such configurations. The contours around the nulls correspond to $|B_p/B_{pm}| = 0.1$.

A full divertor design includes not only the magnetic configuration but also position and shapes of the divertor targets, position of pumping ports and gas-puffs (if used). The same magnetic configuration may give rise to quite different divertor designs. In particular, a tripod configuration of Fig. 5(f) (or adjacent to it topologically stable configurations Figs. 5(e) and 5(g)) may serve as a basis for the Pitts' divertor[30] (where the target would be situated in front of the null), or as a basis for a recently proposed X-point target divertor[74] (where the second null would be enclosed in a separate divertor chamber). This can be done with the underlying snowflake configuration remaining unchanged.

Such divertor designs can be implemented (and the Pitts' divertor has actually been implemented, Ref. 30) with the field structures where the two nulls are situated at a large distance from each other, so that the magnetic configuration does not belong to the snowflake family of Fig. 5. In other words, placing the second null near one of the branches of the main separatrix, far away from the main null, is a feature that is independent and separate from the snowflake approach.

So, when using the terms "quasi-snowflake" and "tripod" to characterise the near-snowflake configurations, one has to exercise caution, as some of the structures mentioned in the previous paragraph may look similar to the ones shown in Fig. 5, but still not belong to the snowflake family. We would not recommend to expand the terms "quasi-snowflake" and "tripod" to describe these configurations.

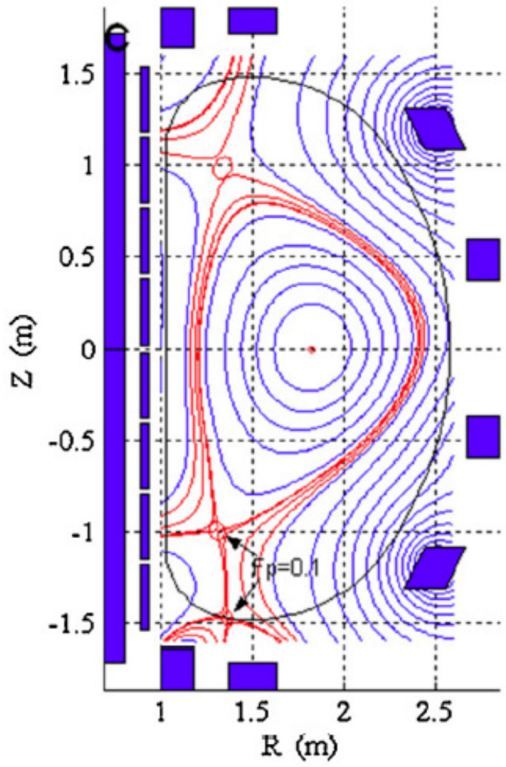

FIG. 7. A tripod magnetic configuration in the lower divertor of the HL-2M facility, courtesy G.-Y. Zheng. This is an almost exact tripod, with the second null lying very close to the main separatrix. Reprinted with permission from Zheng *et al.* Fusion Eng. Des. **89**, 2621 (2014). Copyright 2014 Elsevier.

A direct consequence of generating the field by the remote currents is that the nulls are automatically, by construct, acting in concert with each other: if, for example, we are moving them closer to each other, by manipulating the currents in the PF coils, the field changes significantly around *each* of the nulls, both the "main" one, bordering the confinement zone, and the second one, near which one may want to put the divertor target. One cannot consider the adjustments of the field structures near the second null separately from the changes occurring near the main one. These observations were a trademark of the initial snowflake publications[34,35] and remain the basis for the snowflake divertor analyses to date. The interdependence of the two nulls may be considered as a disadvantage of the snowflake configuration as it would limit divertor design options, but this is a cost that has to be paid for the possibility of creating and controlling the magnetic configurations of the snowflake family by remote coils.

We sometimes speak in this paper figuratively about a "conversation" between the nulls, as this word sends a qualitative message that their mutual position and the distance between them determine the overall field structure. Of course, the field and the positions of the nulls and separatrices are determined by the currents and are the physical entities of their own, not the results of some Taylor series expansions. What these expansions, however, help to highlight is that the structures of the smooth magnetic fields *are constrained* and are fully determined (aside from the field strength) by a simple geometrical parameter ϑ (Fig. 5(d)).

Near each of the nulls of the quasi-snowflakes, at the distances smaller than the distance between the nulls, the field behaves as in the case of a standard divertor, i.e., the absolute value of the field is independent on the direction and scales linearly with the distance from the null in question. Indeed, consider small distances δz from the "main" null, $z = 0$. Equation (10) then shows that $F \approx -A_2 z_2 \delta z$, and

$$B_p = |F| \approx |A_2| Dr, \tag{40}$$

where $D = |z_2|$ is the distance between the nulls, and $r = |\delta z|$ is a (small) distance from the first of them. Consider now the vicinity of the second null and introduce $\delta z = z - z_2$. Then, we again have $F \approx -A_2 z_2 \delta z$ and we recover the same expression for the field variation, with r being now a distance from the second null, $r = |z - z_2|$. The derivatives dB_p/dr are also identical. This property is quite general in the sense that it takes place for any of the configurations shown in Fig. 5. This is the simplest example of a "conversation" between the two nulls: the second null "knows" of the presence of the first null nearby. An approximately equal "flatness" of the field ($|\nabla B_p| = |A_2| D$) in these two nulls is a general property of the field created by remote coils.

The flatness is not a parameter that can be easily found by direct magnetic measurements (although it can be determined via magnetic reconstructions by the equilibrium codes, as it has

been done in Ref. 75, see Fig. 11 of that paper, where the inverse flatness was found as a function of the distance between the two nulls). Still, it is of significant interest, as it shows an extent of the zone of a low magnetic field near each null.

For finite D, the cubic dependence of the magnetic flux vs. Δ_{min} (Eq. (20)) breaks down. For $\Delta_{min} < D$, the field depends on Δ_{min} linearly, and the flux scales as $\Delta^2_{\min}$; for larger distances, the field becomes insensitive to D and the flux scales as $\Delta^3_{\min}$. This issue has been analysed in significant detail in Ref. 34 and, especially, in Ref. 35.

The poloidal magnetic field pressure in the divertor area may affect the plasma convection and other properties of the divertor. From Eq. (10), it is clear that the spatial distribution of this parameter around the line connecting the two nulls is the same for all configurations shown in Fig. 5.

$$\frac{B_p^2}{8\pi} = \frac{|A_2|^2}{8\pi}|z|^2|z - z_2|^2. \tag{41}$$

The iso-contours for the magnetic field pressure are shown in Fig. 8 for the snowflake-minus ($\vartheta = \pi/12$), tripod ($\vartheta = \pi/3$), and snowflake-plus ($\vartheta = 5\pi/12$). Indeed, the pressure distribution is identical, up to orientation of the line connecting the two nulls. With that, the structure of the field lines in terms of the connectivity of various parts of the SOL is quite different. To show this circumstance, the separatrices are overlaid on the iso-contours of the magnetic pressure.

The poloidal magnetic field strength at the mid-point between the nulls, i.e., at $z = z_2/2$, is $B_p = |A_2|D^2/4$. This parameter is the same for all the configurations shown in Fig. 5, provided the distance D is the same.

Although the plasma current in the divertor area is typically small, its presence may have some effect on the field configuration. This issue is discussed in Appendix C.

B. The proximity condition

One simple measure of the closeness of the quasi-snowflake to an exact snowflake that is commonly used in experimental papers, is the ratio

$$\sigma = D/a \tag{42}$$

that normalizes the null-to-null distance to the minor radius. This is a clearly defined and easy-to-comprehend parameter. Certainly, if $\sigma > 1$, it is hard to expect that the snowflake description will be productive (although there may be exceptions).

When σ is less than one, the two nulls are sufficiently close to each other to allow using a two-null representation of Sec. III A and exploit general properties of this representation. One can make one step further and ask a question: "When the two nulls become so close to each other that the plasma behaviour becomes indistinguishable from the one that would take place in an "exact" snowflake, with its $B_p \sim r^2$ field dependence and the hexagonal shape of the separatrix?" To answer this question, we show in Fig. 6 two quasi-snowflake configurations, "minus" and "plus" with the same null-to-null distance D. A green circle with a center at the midpoint between the two nulls has a radius of D, so that the shortest distance from each of the nulls to this circle is $D/2$, and outside this circle, the field structure is close to an exact snowflake.

Let us now consider how some specific plasma phenomenon occurring in the area of the two nulls, e.g., prompt ion loss, is affected by the parameter D. If the prompt loss encompasses a zone of the size D^* (a red circle) exceeding D, then this effect will be only weakly changed by the fact that there is some separation between the nulls. In other words, if the scale of the zone D^* determining some phenomenon in the exact snowflake exceeds the distance of the two nulls D in a quasi-snowflake, then the finite separation between the nulls does not affect the process in a significant way. This condition was called in Ref. 50 "a proximity constraint." This is a qualitative condition, and one has to be careful when using it, but it helps in a general orientation in the problem.

One more example is the effect of the second null on the plasma transport in the common-flux region (SOL). If the second null lies closer to the main null than the SOL thickness, then the magnetic structure in the major part of the SOL will be correctly described by the model of an exact snowflake. Using Eq. (22), one can write the following order-of-magnitude condition for this to happen:

$$D < a(\lambda_q/a)^{1/3}. \tag{43}$$

This is an order-of-magnitude estimate: when this condition is satisfied marginally, one has to be cautious as the heat flux in the SF− divertor may be split roughly equally between two branches (as illustrated by Fig. 5(b) in Ref. 36); how strong the inequality should be in order to allow the use of the model of an exact snowflake depends on the specifics of a particular device. More discussion of this flux splitting is given in Sec. IV. If, however, the condition (43) is held by a

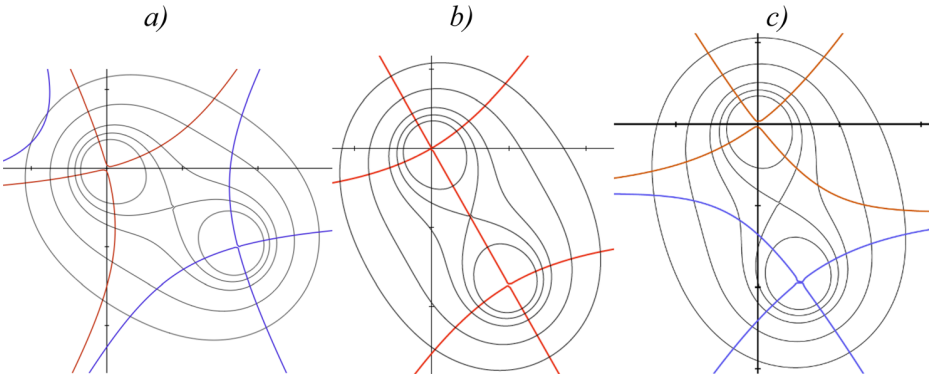

FIG. 8. The isocontours of the magnetic pressure for the SF− (a) a tripod (b) and SF+ (c). The distance between the nulls is the same in all cases. The magnetic pressure distribution is the same, up to a turn of the coordinate frame. On the other hand, the separatrix structure is quite different: in the left panel, the secondary separatrix encloses the primary one (see the segment of the blue line to the left of the main separatrix), whereas in the third case they are separate.

large margin, then essentially all the heat on the outboard side goes to the outermost strike-point, and such parameters of the divertor problem as the SOL volume and connection length become close to those of the exact snowflake. Here, we imply that there is no enhanced transport in a region of a low B_p; the opposite case is discussed in Sec. V.

We see that the proximity to an exact snowflake depends on the specific effect we are interested in: in the aforementioned examples, the proximity constraint may be satisfied for one process and not satisfied for the other.

If the proximity constraint is violated, this by itself does not mean that the general classification of the snowflake field structures of Fig. 5 breaks down—this occurs only when the null-to-null distance becomes comparable to the scale of the global magnetic structure (roughly, when the parameter σ of Eq. (42) becomes $\sim$1). Until D is small in the aforementioned sense, strong interdependence between two nulls exists. This can be seen in a qualitative fashion, by noting that the field structure of each of the panels shown in Fig. 5 possesses a center of symmetry situated in the middle of the red segment connecting the nulls: both nulls are *identical* in the sense of the field structure, up to this reflection.

C. The geometry—experimental results

Experimentally, all the configurations of the snowflake family (Sec. III A) have been produced. Magnetic equilibria reconstructions based on solutions of Grad-Shafranov equations, constrained by magnetic measurements and accounting for kinetic effects, were used in TCV, NSTX, and DIII-D to infer geometric properties of the snowflake configurations. Geometric properties of the snowflake-plus and the snowflake-minus are similar to those of the exact snowflake configuration when the distance D between the poloidal nulls is sufficiently small (Section III B). Figure 9 demonstrates the poloidal field structure in DIII-D.[76] The poloidal flux expansion (35), $(B_pR)^{mid}/(B_pR)^{div}$ evaluated on the divertor target is significantly increased in the snowflake-minus due to the proximity of the target plate to the snowflake. The connection length is significantly increased through most of the SOL radial extent (cf. SOL power width) in the snowflake-minus, and through a smaller fraction of the SOL radial extent in the snowflake-plus. In TCV,[77] the null-region poloidal magnetic flux expansion (see inset in Fig. 5 of that paper) was increased by a factor 1.5–2, the connection length L_c was increased by a factor 2–2.5, for a flux surface whose distance from the separatrix at the midplane was 1 mm. The highest increase in flux expansion and L_c in TCV was obtained with the ideal snowflake configuration. Note that in Ref. 77 the connection length between the midplane and null region was presented, whereas in Ref. 91 the connection length was evaluated between the midplane and the strike-point. In NSTX, the asymmetric snowflake-minus configuration showed an up to 50%–75% increase in L_c and flux expansion in the strike point region. The high flux expansion region extended throughout 30%–50% of the SOL width.

This discussion shows that the flux expansion at the strike point is not an invariant characteristic of the changes in the magnetic geometry. A lot depends on the geometry of the confinement vessel in a particular device. In the practical divertor design, the position and tilt of the target plates (or, speaking more generally, the target plates geometry) would be optimised in coordination with the magnetic geometry.

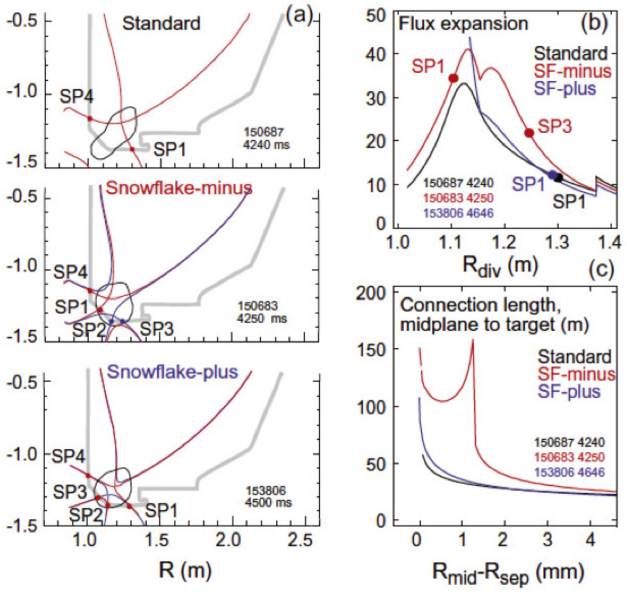

FIG. 9. The snowflake-minus and snowflake-plus divertor configurations realized in DIII-D and comparison of their geometric properties with the divertor configuration with a larger distance between the nulls that is more close to the standard null (SN). (a) Plasma equilibria with the primary (SP1, SP4) and the secondary (SP2, SP3) divertor strike points shown. Also shown are $Bp = 0.1B_p^{mid}$ contours, where B_p^{mid} is the poloidal magnetic field at the midplane separatrix. (b) Radial profiles of $(B_pR)^{mid}/(B_pR)^{div}$ (flux expansion as defined by Eq. (35) and the midplane to target magnetic field line length (connection length) for the three configurations. Reprinted with permission from Soukhanovskii *et al.*,[78] J. Nucl. Mater. **463**, 1191 (2015). Copyright 2014 Elsevier.

The detailed equilibria reconstructions mentioned above are in a good agreement with the two-null representation of Sections II and III A. Fig. 10 shows an example of such a comparison for the snowflake-minus configuration on NSTX.

When assessing the geometrical properties of a snowflake, one should exercise some caution with parameter σ, Eq. (40): in two facilities with different global magnetic configurations, the same value of the parameter σ may not mean that the field properties are the same: what is also important, beside the value of σ, is the coefficient K_2 (Eq. (18)) that characterizes the global structure of the magnetic field and may be different between two facilities or two different global configurations.

If one is interested in the connection length, or magnetic shear, or other similar characteristics of the quasi-snowflake, one has to evaluate them, strictly speaking, separately for different zones in the xy plane. For example, in the case of a snowflake-minus, these would be the zones marked as I–VI in Fig. 11. Within each zone connected to the mid-plane, this has to be done as a function of the distance from the separatrix in the midplane, as this has been done in Fig. 9(c). Such studies have been done in a number of cases related to specific experimentally realized or planned configurations (e.g., TCV,[77] NSTX,[52,79] DIII-D,[76] FAST,[80] HL2-M,[73] and EAST[81]), and we will not dwell on these design-specific

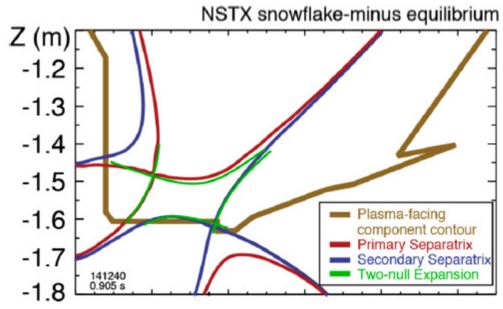

FIG. 10. An overlay of the full equilibrium reconstruction (the red and blue being the primary and secondary separatrices, respectively), and the two-null representation (green). Reprinted with permission from Phys. Plasmas **21**, 054701 (2014). Copyright 2014 AIP Publishing LLC.[78]

calculations. We will, however, note that if the two nulls are situated close-enough to each other, one can ignore their separation and use the estimates of Sec. II B pertaining to the "exact" snowflake. We addressed this issue in general terms in Sec. III B and will later specify conditions for specific divertor effects.

D. Equilibria and control

Tokamak real-time plasma feedback control systems have matured in recent years significantly, leading to the possibility of controlling many critical tokamak plasma parameters, e.g., β, rotation, pedestal structure, and divertor radiation.[82] The desirability of the snowflake divertor configuration control, e.g., the tracking of the two poloidal field nulls and keeping them close to each other in real time with feedback on the magnetic coils, has been emphasized in the initial experimental papers.[52,79] This could be particularly important for maintaining the desired configuration during transients and off-normal events.

Initial tokamak experiments, however, used pre-programmed magnetic coil current targets that satisfied snowflake equilibria designed off-line using free-boundary Grad-Shafranov equilibria solvers. A plasma shape with the standard divertor was taken as the target and the divertor coils currents were iteratively modified to obtain the desired divertor configuration. In some cases, e.g., in TCV, numerical optimization was used to minimize perturbation to the poloidal magnetic flux in the main plasma, and produce minimal deviations of the coil currents from the standard divertor.[77] In the experiment, the obtained coil currents were entered before the discharge into the plasma control system. An iterative approach was again used to fine-tune the configuration in the experiment. A hybrid approach was also possible: in NSTX and DIII-D, the plasma control system was used to control the strike point or main X-point positions in combination with pre-programed coil currents. These techniques enabled snowflake-plus and snowflake-minus configurations for many plasma energy confinement times, sufficient for snowflake divertor studies in the TCV, NSTX, and DIII-D tokamaks using the existing poloidal coil sets. Further optimization of these techniques, still based on static equilibria modeling, has been proposed and implemented for a given set of poloidal field coils, or for a coil set specifically optimized for the snowflake configuration.[81,83]

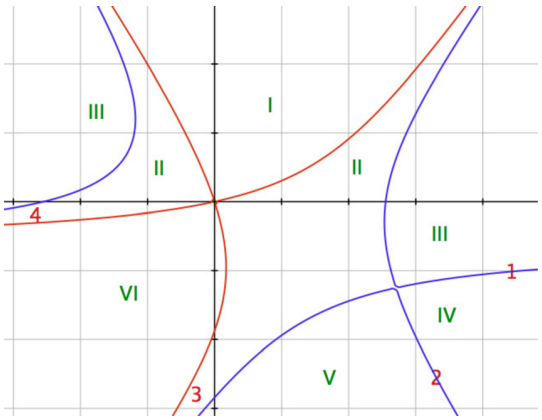

FIG. 11. Partition of the poloidal cross-section by the primary and secondary separatrices for the SF-minus case (Roman numerals). The left and right parts of the domain II and III are connected over the upper part of the confinement region I. The red Arabic numerals designate the four divertor legs.

Long-pulse plasma discharges in present day tokamaks are likely to introduce time-varying magnetic and plasma boundary parameters, e.g., slowly varying divertor magnetic leakage flux due to the time-evolving ohmic solenoid current, or fast plasma pressure variations due to edge localized modes. This necessitates a magnetic feedback control of the divertor configuration. A computationally fast poloidal null tracking algorithm was proposed[84] based on the analytic Grad-Shafranov equation expansion and evaluation of local magnetic field components in real time[85] An application of this algorithm for snowflake divertor configuration control was studied in the DIII-D tokamak. The metrics of the snowflake divertor were the inter-null distance and the orientation of the segment connecting the nulls, in accordance with the proposed snowflake classification schemes.[36] The coil currents needed for a desired snowflake configuration were calculated in real time by finding the linearized effect of the coil currents on the snowflake configuration parameters at every instance using real-time EFIT. The power supply system was controlled to achieve the desired currents using a proportional integral-derivative controller. These promising results are an initial step in the snowflake divertor control and optimization development for existing and future tokamaks.

IV. SCRAPE-OFF LAYER FOR THE NEAR-SNOWFLAKE CONFIGURATIONS

A. Qualitative analysis

We now qualitatively discuss how the finite distance between two nulls can affect the structure of the scrape-off layer and the partition of the heat flux in the quasi-snowflakes. This discussion can serve as a template for assessing the role of the finite D in other phenomena summarized in Sec. II C. We will focus on the SOL plasma transport on the flux surfaces directly connected along the field lines to the mid-plane SOL, a standard procedure for an initial qualitative analysis of the divertors.[11] Later, in Sec. V, some additional mechanisms of the plasma transport in the

zone of a weak poloidal field and to the private flux region will be considered.

Assume first that the distance between the nulls is significantly smaller than the SOL thickness at the point of the maximum flux flaring (Eq. (22)). We denote this thickness by Δ_{div} to distinguish it from the running parameter Δ_{min}, with $\Delta_{min} = \Delta_{div}$ at the SOL boundary [In reality, the SOL does not have a step-wise boundary, so that Δ_{div} has a qualitative meaning of a "characteristic" width.]. Assume, therefore, that

$$D \ll \Delta_{div}. \tag{44}$$

(Figs. 12(a) and 12(b)). The field structure over the most part of the SOL near the null is then essentially the same as for the exact snowflake (see Sec. III B), and this would be correct for all the structures shown in Fig. 5, including snowflake-plus and snowflake-minus (where only a small fraction of the plasma flux is diverted to the additional strike point). Equation (44) becomes then $D \ll a(\lambda_q/a)^{1/3}$, where a is the minor radius and λ_q is the SOL power width projected to midplane (cf. Eq. (43)). Issues of the plasma penetration to the private flux region require a separate analysis; in the absence of some additional, snowflake-specific, modes of the transport in the weak B_p region (discussed in Sec. V), the plasma penetration to the private flux region is typically modest, in agreement with recent simulations of Ref. 90.

As mentioned, with the same (small) values of σ, condition (43) may be satisfied in one machine and not satisfied in the other, due to possible different midplane SOL thickness Δ and different value of the parameter K_2 in Eq. (18).

When the distance D becomes comparable to Δ_{div}, there may appear significant difference between the SF+ and SF−, as illustrated in Fig. 12. Assume, for example, that the distance D is about half of Δ_{div}, Figs. 12(c) and 12(d). Then, in the case of a SF−, there will be heat flux splitting between two divertor leg's 1 and 3 (Fig. 12(c)), whereas in the case of SF+ (Fig. 12(d)), the heat flow will still go to the same strike point. Here, we assume first that the field structure is not perturbed by the presence of the plasma, as is the case for a low-beta plasma, and that only small fraction of the total heat and particle flux penetrates to the private flux region—a typical situation for the standard divertors. Under the same assumption, in a SF+ geometry of Figs. 12(d) and 12(f), only the private flux region is diverted to the additional strike point.

As mentioned in Ref. 36, the configuration of Fig. 12(c) may serve as a basis for the divertor with two strike points for the outer SOL. A much more detailed analysis of this possibility, involving an optimization of the divertor configuration, was presented in Ref. 86.

If D becomes greater than Δ_{div}, the heat and particle flux go to quite different strike-points, 1 for the SF+ and 3 for the SF−. A broad range of configurations that are controlled by the remote coils opens up a number of design choices for divertor configurations. Note that characterizing divertor by the position of the divertor plate with respect to the second null may be confusing, especially when multiple divertor channels are activated.

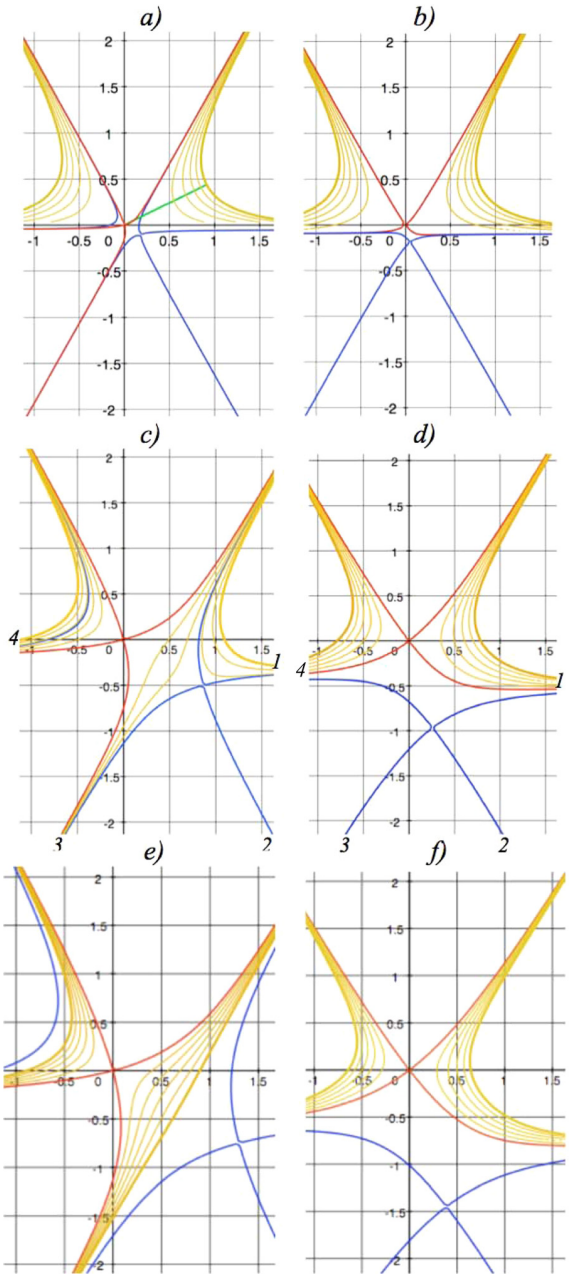

FIG. 12. Scrape-off layer for different distances between the two nulls. Left columns corresponds to the SF− ($\vartheta = \pi/6$); right column corresponds to SF+ ($\vartheta = 5\pi/12$). Red lines depict the main separatrix; blue lines, the secondary separatrix. Bold yellow line shows the SOL boundary (the same flux in all cases). The minimal distance between the main null and the nearest point at the SOL boundary in the upper row is 1. The distance D between the nulls in the same units is 0.2 in the upper row, 1.4 in the middle row, and 2.5 in the lower row. The numbers in the second row indicate possible strike points in the nomenclature of Fig. 11. In the first case, the difference between the "−" and "+" configurations is negligible. In the second case, the secondary separatrix for the SF− cuts the SOL roughly "in halves;" the outboard SOL heat flux is shared roughly equally between two divertor legs, 1 and 3. In the SF+ case, the outer heat flux still goes only to SP 1 (neglecting a "leakage" to the private flux region). In the lower row, the difference becomes even more significant: in the SF− case, all the heat flux goes to SP 3, whereas for the SF+, it goes entirely to SP 1. We emphasize that this analysis relates to the standard SOL assumptions: small effect of the plasma on the field structure, plus small leakage to the private flux region.

The SF− field configuration shown in Figs. 12(c) and 12(e) can have an interesting effect on the propagation of the SOL filaments ("blobs," Ref. 62): when moving in the

outward direction, the filament would have to cross the secondary separatrix and experience a break at the null (Fig. 13). This may be of some significance for the wall erosion caused by blobs. This effect, however, has not been yet explored either theoretically or experimentally.

B. Numerical simulations

In our discussion below, we assume that the field is static and well characterized by the vacuum expansions. This is typically a setting used in the 2D simulations of the plasma transport in the codes like UEDGE[87,88] and SOLPS.[89] Significant number of numerical studies of the plasma transport in snowflake divertors has been produced.[51–58] Most of them used 2D transport codes and were focused on effects occurring in the two divertor legs adjacent to the main separatrix. The features of the snowflake geometry that had strong effect on the plasma behaviour included the flux flaring and increased connection length (related to the SOL volume near the null, see Sec. II B). The neutral behaviour was an important factor. A general conclusion of these studies was that, under the comparable conditions, the use of the snowflake divertor allows one to significantly reduce the maximum heat flux.

These studies addressed the existing devices, like DIII-D (Ref. 51), TCV (Ref. 90), and NSTX (Ref. 52), as well as the planned ones, like NSTX-U (Ref. 55), FAST (Refs. 54 and 56), DEMO (Ref. 57), and CFETR (Ref. 58). In some cases, the reduction of the heat flux was greater than related only to flux expansion;[51] this was attributed to radiation and change in the neutral penetration to the SOL plasma.[51]

Most of these studies covered the steady situations. Temporal effects occurring during ELMs have been simulated in Ref. 53. It was shown that the increased connection length leads to a temporal "stretching" of the ELM heat pulse on the divertor target, leading to reduction of the instantaneous heat load and decrease of the temperature excursion.

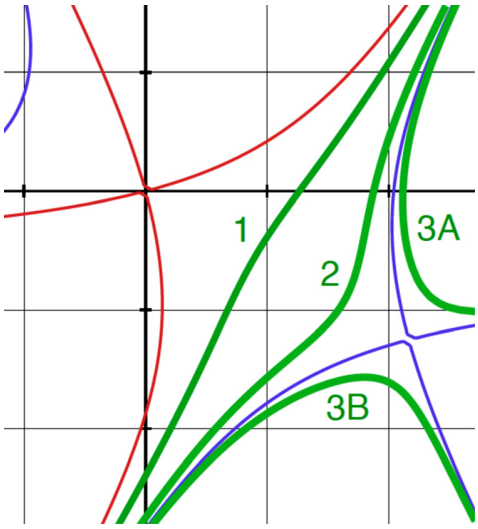

FIG. 13. The blob (shown in green) propagating in the outboard direction in the snowflake-minus configuration, from position 1, to position 2, and further to position 3. When passing through the secondary null, it has to split into two independent structures, A and B. This splitting will affect the further propagation of the structure 3A to the wall and structure 3B in the divertor region. For a better visibility, we take a large distance between the two nulls, but the same effect would occur at a smaller distance as well. Note that in a full three-dimensional picture the blob looks as a filament winding around a plasma; we show here a projection of the blob onto poloidal plane.

As mentioned, these studies were considering the two outer divertor legs directly connected to the upper SOL and, therefore, could not assess the "activation" of additional strike points. The first numerical analysis of a full geometry, with all the branches of the separatrices included, was performed by Lunt *et al.*[90] The transport coefficients were adjusted to fit the SOL width for the two outer divertor legs, and then, with the same transport coefficients, the simulation was made for the whole domain for the SF+ geometry. This important study based on the EMC3-Eirene transport code was the first one where a real quasi-snowflake divertor geometry with multiple topologically separated zones has been performed. The conclusion was reached that the transport coefficients that correctly describe the SOL in the common flux region are by far insufficient to produce significant spreading of the plasma and heat flux across the multiple separatrices. The code strongly underpredicts (by at least an order of magnitude) the experimentally observed (see Sec. IV C) amount of heat penetrating to additional strike points. So, some strong additional mechanisms have to be included to explain the experimentally observed heat flux spreading. One candidate is particle drifts that were not included in the current simulation. We discuss this and other possible candidates for the enhanced transport in Sec. V.

C. Experimental studies of transport and turbulence in the upper SOL and divertor

The effects of the snowflake divertor configuration on scrape-off layer transport and turbulence are multifaceted, as described in Section IV A. In the experiments, directly measured quantities, e.g., inter-ELM and ELM heat and particle fluxes and fluctuations, are clearly different in the snowflake configuration (cf. standard divertor); however, unambiguous interpretations are often too complicated.

Some measurable effects on fluctuations and blobs have been observed in TCV L- and H-mode plasmas with the snowflake-plus configuration using Langmuir probes (Fig. 14). The frequency of density blobs measured via conditionally sampled probe ion saturation currents on the low field side midplane was much greater in the standard divertor configuration, suggesting either a faster parallel convection or blob suppression by high magnetic shear in the snowflake configuration mentioned in Sec. II C (see Refs. 64 and 65).

Divertor transport was systematically studied in TCV. Heat fluxes in all strike points were compared between the standard and snowflake configurations in both the L-mode and H-mode (inter-ELM and ELM) discharges. As mentioned in Sec. III, the heat flux sharing between two strike-points connected to the upper SOL by geometrical effect present in the snowflake-minus configuration may occur in a "natural way" without participation of any other effects but the flux surface geometry (see left column in Fig. 12). On the other hand, the flux sharing between multiple strike

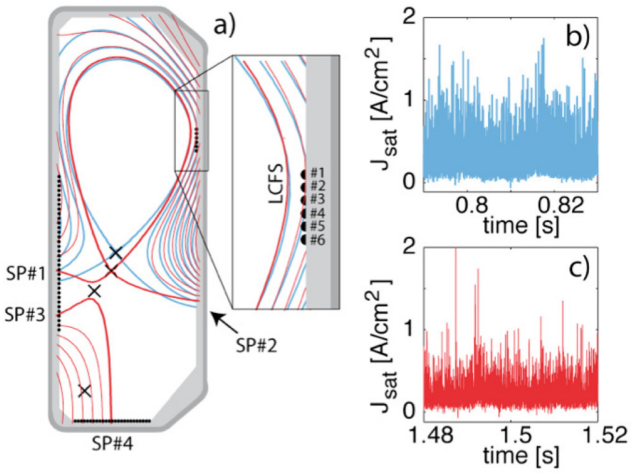

FIG. 14. (a) Plasma equilibria for the standard divertor (blue) and snowflake-plus (red) configurations in the TCV tokamak with Langmuir Probes #1–#3 in the scrape-off layer (see an inset to the right of panel (a)). Examples of measured J_{sat} in the standard divertor phase (b) and the snowflake-plus (c) configurations. Courtesy B. Labit. Reprinted with permission form Labit *et al.*, in *2010 IAEA Fusion Energy Conference, Daejoen, Korea* (International Atomic Energy Agency, Vienna, 2010), Paper No. EXC/P8-08.[64]

points in a snowflake-plus geometry requires some mechanisms for the heat and particle transport across the vacuum separatrices, see right column in Fig. 12.

To isolate the effect of plasma transport across the separatrices, a set of experiments was performed on TCV where the field structure would be of a snowflake-plus type. The appearance of heat in the additional strike points ("strike point activation") was studied as a function of the distance between poloidal field nulls, Fig. 15. In L-mode, finite, but small, heat flux was observed in the additional strike points. In contrast, heat fluxes during type I ELMs are significantly shared between multiple strike points: e.g., the particle and heat fluxes in the primary strike points were substantially reduced by 50%–75%. Between ELMs, a large reduction, up to 50%, of heat flux to the primary strike points was also observed, with a significant fraction going to the secondary strike points.[75,91] This may suggest an enhanced transport mechanism that carries the heat across the null-region magnetic field lines.

In DIII-D, lower peak target temperatures and reduced heat loads (cf. standard divertor) due to ELMs were measured in the snowflake configurations. The increased divertor connection length L_c can reduce the target surface temperature rise ΔT due to pulsed heat load during an ELM according to $\Delta T \sim (\tau_d)^{-1/2} W_{ELM} A_{wet}$, where W_{ELM} is the ELM energy, A_{wet} is the wetted area, and τ_d is the ELM deposition time which is increased at longer L_c. This effect was also captured in the UEDGE simulations.[53] Another possible mechanism is the fast plasma transport in the low B_p region driven by a variety of mechanisms discussed in Sec. V below and leading to the ELM heat flux sharing among the additional strike points. The peak powers were reduced in the snowflake-minus by up to 50%–70%, and further reduced in the radiative SF-minus by up to 50% (cf. standard divertor configurations).

In the NSTX radiative snowflake-minus configuration, the heat fluxes from Type I ELMs were significantly dissipated from about 20 MW/m^2 (from an ELM in the standard divertor phase of the discharge) to 6–8 MW/m^2 during the snowflake formation phase and eventually below 2 MW/m^2 in the radiative snowflake phase (Fig. 16). Peak target temperatures at peak ELM times, as measured by infrared thermography, reached 1000–1200 °C in the standard divertor

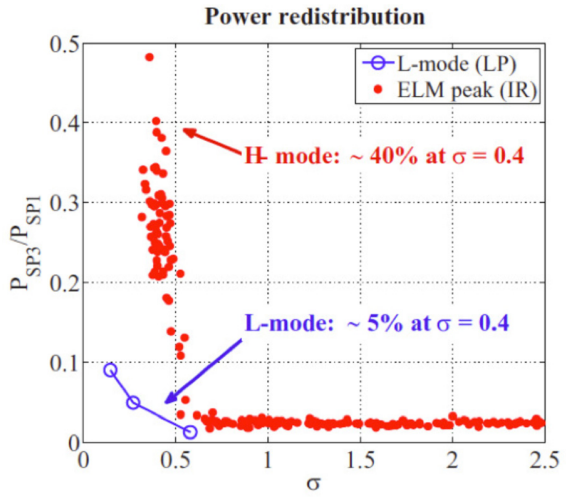

FIG. 15. Power redistribution in the snowflake-plus divertor configuration in TCV. The power fraction P_{SP3}/P_{SP1}, a ratio of divertor power measured in the strike points SP4 and SP1 in Fig. 14 (note the different numbering in the current figure), as a function of σ in both L-mode and at the ELM-peak in H-mode. Courtesy W. A. J. Vijvers. Reprinted with permission from Vijvers *et al.*, Nucl. Fusion **54**, 023009 (2014). Copyright 2014 International Atomic Energy Agency.

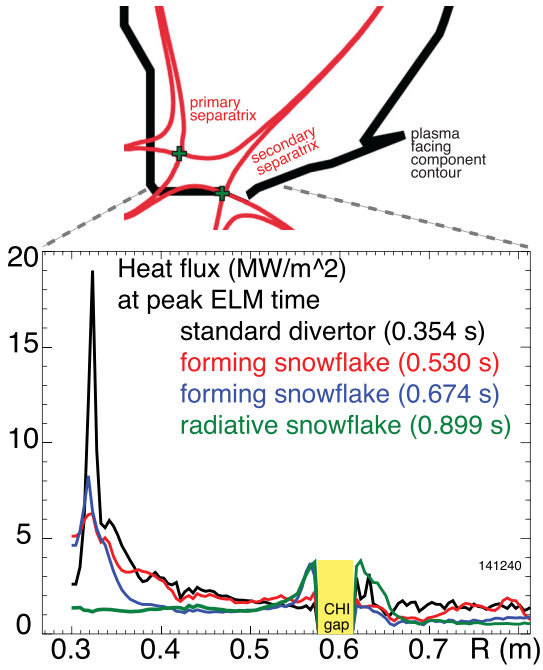

FIG. 16. Divertor heat flux profiles measured by IR thermography at peak ELM times in NSTX before and during the snowflake-minus formation, as well as in the radiative snowflake-minus phase. Reprinted with permission from J. Nucl. Mater. **438**, S96 (2013). Copyright 2013 Elsevier.

and only 300–500 °C in the snowflake phase. During ELMs, an additional peak in the heat flux (and temperature) profile at the secondary strike point location (and also where f_{exp} and L_X were similar to that of the standard divertor) was evident. The ELM heat flux profiles were consistent with power sharing between the primary and secondary strike points.

The standard modelling of the divertor based on the ansatz of approximately constant cross-field transport coefficients has been thoroughly studied numerically by Lunt *et al.*,[90] see Sec. IV B. The conclusion was reached that the transport coefficients that correctly describe the SOL in the common flux region are by far insufficient to produce significant spreading of the plasma and heat flux across the multiple separatrices. So, some strong additional mechanisms have to be included to explain the experimentally observed heat flux spreading. We consider them in Section V.

V. POSSIBLE MECHANISMS FOR THE POWER SHARING

A. $E \times B$ drifts

The $\boldsymbol{E} \times \boldsymbol{B}$ drifts in quasi-static electric fields in SOL and divertor area have been identified as a factor that may significantly affect the performance of a standard divertor, e.g., Refs. 92–94. They could be of significance in the snowflake divertor as well. In particular, they may cause the plasma transport across the plasma separatrices, as emphasized by Canal *et al.*[48] The velocity of the electric drift is

$$\mathbf{v}_E = c\frac{\boldsymbol{B} \times \nabla\varphi}{B^2}. \tag{45}$$

In a 2D problem of a SOL transport, with the toroidal direction being an ignorable coordinate, the component of the drift velocity across the flux surface is related to the poloidal variation of the electrostatic potential

$$\mathrm{v}_{En} = \frac{c}{B_T}\frac{\partial\varphi}{\partial l}, \tag{46}$$

where the subscript "n" means the normal to the flux surface, and $\partial\varphi/\partial l$ denotes the derivative along the poloidal field. We have used here an approximation $B = \sqrt{B_T^2 + B_P^2} \approx B_T$.

Consider possible contribution of this effect on the plasma penetration to additional strike points for the SF+ geometry (Fig. 12, right column). The time that a parcel of plasma spends to travel the distance dl in the poloidal direction is

$$dt = (B_T/B_P)dl/\mathrm{v}_{\|}. \tag{47}$$

Within this time, a parcel moves from one flux surface to another, with a poloidal field flux different from the initial one by

$$\begin{aligned} d\tilde{\Phi} &= 2\pi R B_p \mathrm{v}_{En} dt = 2\pi R B_T (\mathrm{v}_{En}/\mathrm{v}_{\|}) dl \\ &= 2\pi R c(\partial\varphi/\partial l)(dl/\mathrm{v}_{\|}) \end{aligned} \tag{48}$$

($\tilde{\Phi}$ in this section is the flux between two poloidal flux surfaces over the whole toroidal circumference; it should not be confused with the flux Φ per unit length in the toroidal direction, cf. Sec. II B). If the divertor is in the attached regime, the parallel flow velocity does not change significantly and is on the order of the sound speed c_s. The major radius in the divertor zone also does not change much. Then, one can integrate Eq. (46) from point a to point b in the poloidal cross-section to find that the drift has caused a shift of the parcel by

$$\delta\tilde{\Phi} \approx 2\pi R c(\delta\varphi)_{ab}/c_s. \tag{49}$$

This is quite a universal result, applicable to both standard and snowflake divetor. Assuming that $e(\delta\varphi)_{ab}$ is a fraction α of the electron temperature $e(\delta\varphi)_{ab} \sim \alpha T_e$, we find that

$$\delta\tilde{\Phi} \approx 2\pi R\frac{\alpha c T_e}{e c_s}. \tag{50}$$

The coefficient α depends on the details of the model. Expression (50) has to be compared to the magnetic flux enclosed between the two separatrices defined by Eq. (39). Assuming that in Eq. (39), $\sin\vartheta \sim 1$, $K_2 \sim 1$, we find that significant penetration of the plasma to the secondary separatrix (i.e., $\delta\tilde{\boldsymbol{\Phi}} > \tilde{\boldsymbol{\Phi}}_{12}$) would occur if

$$\frac{D}{a} < \left(\alpha\frac{cT_e}{eB_{pm}ac_s}\right)^{1/3}. \tag{51}$$

Taking $\alpha \sim 0.1$, one finds that for a typical tokamak SOL with $T_e \sim 50$ eV, this condition is satisfied if $D/a < 0.1$.

The penetration through the second separatrix would not necessarily change the parallel flow velocity. In the geometry of, say, Fig. 5(i), the plasma may still flow to the same divertor target even after crossing the second separatrix. To find an actual partition of the plasma flow between the strike points needs significantly more detailed analysis.

One more comment that is appropriate here is that condition $\mathrm{v}_{||} \sim c_S$ is based on the assumption that poloidal projection of the parallel velocity is higher than poloidal drift velocity $\mathrm{v}_{EP} = c(\partial\varphi/\partial n)/B_T$, where $\partial\varphi/\partial n$ means the derivative along the normal to the flux surface (cf. Ref. 92). One has $\mathrm{v}_{EP} = c(\partial\varphi/\partial n)/B_T = 2\pi R B_p c(\partial\varphi/\partial\tilde{\Phi})/B_T$, so that the ratio of v_{EP} to the poloidal projection of the parallel velocity, $\mathrm{v}_{\|}B_p/B_T$, can be presented (for $\mathrm{v}_{\|} \sim c_s$) as

$$\sim\frac{2\pi R c\left(\partial\varphi/\partial\tilde{\Phi}\right)}{c_s}. \tag{52}$$

As the normal potential difference over the SOL is of order of T_e/e along the whole SOL, one sees that this ratio remains roughly constant over the divertor area, including the zone of strong flux expansion near the main null. The flux enclosed by the SOL can be represented as $2\pi R B_{pm}\Delta_m$, this leading to the following form of the ratio (52):

$$\sim\frac{cT_e}{eB_{pm}\Delta_m c_s}. \tag{53}$$

This ratio is typically of the order of 0.3–0.5, so that the drift correction to the poloidal flow velocity may be non-

negligible. For the outer SOL, this velocity adds up with the parallel flow velocity and leads to some decrease of the drift effects. For the inner leg, however, this velocity is directed against the parallel flow and may enhance the effect.[48] One has to remember that for the toroidal magnetic field in the "standard" direction (i.e., for toroidal drift directed downward), the normal component of the drift velocity is directed away from the separatrix. Therefore, the toroidal magnetic field reversal may give rise to significant change in the electrostatic convection.[48,49]

B. Magnetic field stochastization

There have not been any detailed studies of the magnetic stochasticity for the snowflake divertor, aside for a general comment in Ref. 95 (see Eqs. (7) and (22) of that reference). An important difference between the standard divertor and snowflake or near-snowflake configurations is the presence of an area of a very weak poloidal magnetic field. Due to a strong divergence of the q factor (see Sec. II) in the snowflake case, the resonances will be tightly spaced, leading to an easier onset of the stochasticity.[96] A consistent analysis of this problem, especially in a setting with two separate nearby nulls, is still in the future. Potentially interesting effects may come from the coupling of the snowflake magnetic field with deliberately imposed magnetic perturbations, similar to what is done in standard divertors.[97]

C. A "churning mode"

Potentially important mechanism for the plasma spreading between the four strike points has been identified in Ref. 71 and is related to onset of the 2D (toroidally symmetric) plasma convection near the snowflake poloidal field null, in the zone where the poloidal field pressure is comparable to or smaller than the plasma pressure, so that $\beta_p \equiv 8\pi p/B_p^2 \gg 1$. To get some insight into the possible consequences of this situation, assume for a while that the poloidal field is absent in this zone. The plasma equilibrium condition then would read

$$\nabla p = \boldsymbol{j}_p \times \boldsymbol{B}_T/c, \tag{54}$$

wherefrom we find that $\boldsymbol{j}_p = c[\boldsymbol{B}_T \times \nabla p]/B_T^2$. Using standard equations of the vector analysis and noting that $B_T \propto 1/R$, $\nabla \times \boldsymbol{B}_T = 0$, we get

$$\nabla \cdot \boldsymbol{j}_p = -\frac{c}{RB_T}\frac{\partial p}{\partial y}. \tag{55}$$

In the toroidally symmetric case, $\nabla \cdot \boldsymbol{j}_p = 0$, this meaning that, in any area where there is a vertical plasma gradient ($\partial p/\partial y \neq 0$), the plasma equilibrium in a purely toroidal field is impossible. If the vertical gradient is present, plasma starts moving and condition $\nabla \cdot \boldsymbol{j}_p = 0$ is recovered via the onset of acceleration and the corresponding polarisation currents.

As the plasma pressure in the divertor area experiences a general variation from higher pressures above the null to lower pressures below it (in the geometry of Fig. 17), there is no plasma equilibrium and plasma convection develops. Note that the presence of the finite *radial* gradient ($\partial p/\partial x \neq 0$) is consistent with the plasma *equilibrium*. The radial gradient, if negative (pressure decreases away from the geometrical axis) can, however, drive plasma *instabilities* that we consider in Sec. V D.

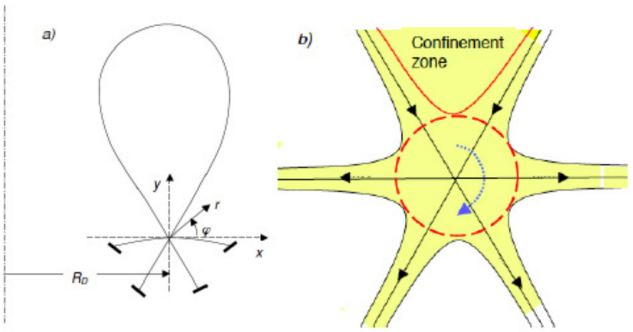

FIG. 17. The geometry of the system for the case of a snowflake divertor: (a) the overall configuration; the divertor targets (bold lines) are situated at the ends of the four outgoing branches of the separatrix; (b) the structure of the weak poloidal field zone near the null; black arrows indicate the direction of the plasma flow; dashed red circle encloses the convection zone with blue dashed arrow indicating the initial direction of rotation; solid red line inside the confinement zone shows the boundary of a layer inside the separatrix affected by convection; in the equatorial plane, this layer becomes quite narrow, see Eqs. (22) and (23). Reprinted with permission from Ryutov *et al.*, Ref. 71 Phys. Scr. **89**, 088002 (2014). Copyright 2014 The Royal Swedish Academy of Sciences. Reproduced with permission from IOP Publishing. Copyright IOP Publishing.

The origin of convection is basically the same as in the usual fluid in the gravity force: Imagine a box filled with a fluid and heated from one of the side walls (not from the bottom). The fluid near the wall expands and, driven by the buoyancy force, starts flowing upward, turning in the horizontal direction near the top, flowing along the upper surface, and going down on the opposite (cold) side wall (baroclinic convection). A convection cell then appears and is sustained for as long as the temperature difference between the side walls is maintained.[98] In our case, the situation is quite similar, just turned by 90°: the effective gravity is directed horizontally, and the fluid is heated from the top.

The poloidal magnetic pressure for the snowflake grows as the 4th power of the distance from the null and, being negligibly small in the vicinity of the null, sharply increases at larger distances and provides a counteraction to the just described "churning" motion. One can, therefore, expect that the plasma convection will appear only in some limited area near the null, whereas at larger distances from the null, a standard plasma equilibrium will be re-established. The size of the zone affected by convection was estimated within a heuristic model of this "churning mode," where the energy arguments have been used: the energy release by an expanding plasma parcel moving to a larger major radius is balanced by the increase of the poloidal magnetic field energy caused by the twisting of this field[71] [Note a typo in Eq. (20) of Ref. 71, where there should be d^{2n+2} instead of d^{n+2}; this typo does not propagate to further equations.]

The schematic of a churning mode for the snowflake case is shown in Fig. 18. A similar effect for the standard

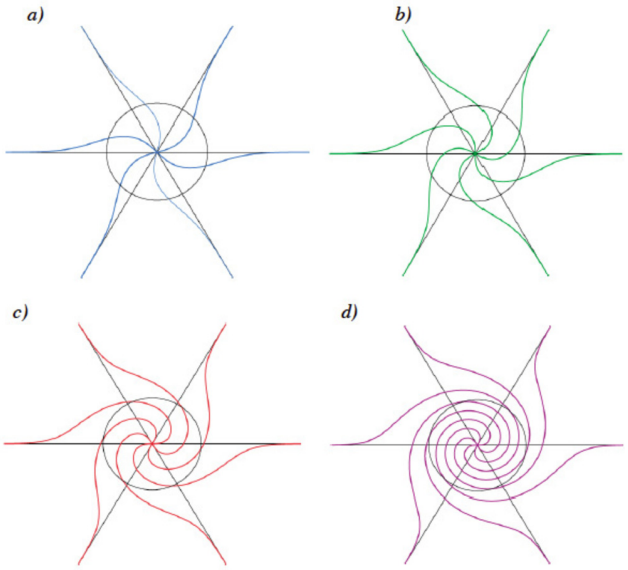

FIG. 18. Evolution of the separatrix entrained by the churning mode. The coordinates are normalized to d, with the circle having a radius of the unity. Black straight lines indicate six branches of the unperturbed snowflake separatrix. The upper left panel corresponds to the near-axis twist (χ) of $\pi/4$, upper right panel, to $\chi_0 = \pi/2$, the lower left panel corresponds to the upside-down turn $\chi_0 = \pi/2$, and the lower right panel corresponds to a stronger drive, where a full 2π turn becomes possible. The cross-field transport is strongly facilitated for the lower two panels due to the significantly shortened cross-field scale. Reprinted with permission from Ryutov *et al.*, Phys. Scr. **89**, 088002 (2014). Copyright 2014 The Royal Swedish Academy of Sciences. Reproduced with permission from IOP Publishing. Copyright IOP Publishing.

divertor would be much weaker due to higher values of the poloidal field. In the case of a snowflake, the radius D of the convective zone vs. midplane poloidal beta, β_{pm}, was evaluated in Ref. 71 (with a corrected numerical coefficient) as

$$\frac{D}{a} \approx 0.81\left(\beta_{pm}\frac{a}{R}\right)^{1/3}. \tag{56}$$

For the generic mid-size tokamak with parameters mentioned in Table II, the ratio D/a for a snowflake divertor is $\sim$1/10. For a fusion reactor of ITER scale, the radius D of the convection zone will be $\sim$20–30 cm. The dependence of the size of the convection zone on the separation between two nulls in the case where this separation is comparable to or greater than the size (56) is still a matter for the future studies.

D. MHD instabilities and MHD turbulence

Plasma redistribution between the divertor legs can also be caused by curvature-driven MHD instabilities, in the case

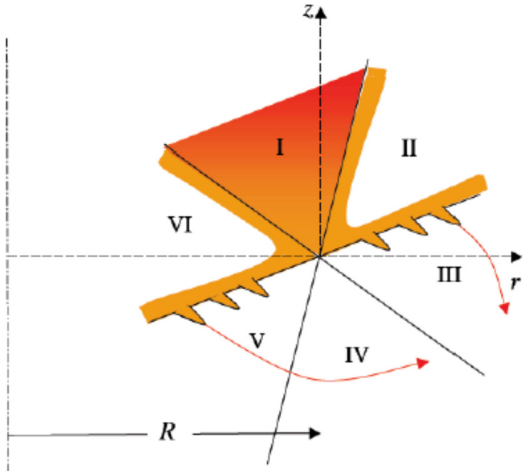

FIG. 19. Assuming that the SOL plasma does not penetrate to the private flux region diffusively, one finds that, for the snowflake orientation shown in this figure, the lower boundary is unstable with respect to toroidally symmetric flute-like perturbations that should cause a plasma penetration to zones III and V. Note that this figure depicts the inward tilt of the snowflake configuration, whereas Fig. 4 corresponds to the outboard tilt, and conceptual Figure 17 to no tilt at all.

where the pressure decreases toward weaker toroidal field. This mechanism is illustrated by Fig. 19 (Ref. 99). Assume that initially plasma is present only in the common flux region of the SOL. Then, the interfaces of the SOL with zones III and V for the snowflake oriented as shown in this figure may become unstable (as shown by the ripple on the interfaces). In order not to perturb the strong toroidal magnetic field, the perturbations have to be toroidally symmetric or nearly toroidally symmetric. If present, these modes have high growth rate and may lead to spreading of the plasma in the direction of the arrows shown in Fig. 19.

The first group of modes that can be called a flute mode with respect to toroidal magnetic field has been considered in Ref. 70(a). These modes do not perturb toroidal magnetic field but may perturb the weak poloidal field. To make the perturbation of the poloidal field minimal, these modes favour small poloidal mode numbers and may be sensitive to the boundary conditions on the target plates. In the analysis of Ref. 70(a), the perfect line-tying conditions have been imposed, this leading to a relatively high instability threshold. A conclusion was drawn that these modes can develop during the ELM events, when the plasma pressure in the SOL increases significantly. Accounting for the presence of the sheaths may lead to a relaxed line-tying and reduction of the threshold. In the same direction would act possible detachment.

Ballooning modes have been considered in Ref. 70(b), with the similar conclusion regarding the threshold.

TABLE II. Parameters of a generic mid-size tokamak used in the numerical estimates.[a]

Parameter	Major radius	Minor radius	Toroidal field	Midplane poloidal field (PF)	Plasma dens. in conv. zone	Plasma temp. in conv. zone
Notation	R, cm	A, cm	B_T, T	B_{pm}, T	n, cm^{-3}	T, eV
Value	150	60	2	0.25	10^{13}	50

[a]Reprinted with permission from Ryutov *et al.*, Ref. 71 Phys. Scr. **89**, 088002 (2014). Copyright 2014 The Royal Swedish Academy of Sciences. Reproduced with permission from IOP Publishing. Copyright IOP Publishing.

Magnetic shear may lead to a stabilizing effect.[70(b)] All this area needs more detailed study. In particular, neither analytical nor numerical studies of the developed stages of these instabilities are available at present.

The mechanisms of the heat flux sharing identified above are dependent on the details of the geometry: in particular, the pressure-driven convection of Sec. V C and the MHD turbulence of Sec. V D are sensitive to the orientation of the separatrix branches with respect to the geometrical axis. So, their manifestations may be different for the facilities with similar plasma parameters but with different orientation of the flux surfaces. Another set of effects not yet considered in any detail is the possible role of the non-MHD physics.

VI. PROMPT ION LOSSES AND NEOCLASSICAL ION ORBITS

Continuing discussion of the plasma physics effects impacted by the snowflake, we dwell now on the ion orbit effects. To be specific, we consider the situation where the ion magnetic drift is directed downward in the geometry of Fig. 1. In this case, there exists a mechanism for prompt (single-orbit) ion losses from the vicinity of the separatrix. This mechanism has been identified for the standard divertors in Refs. 67 and 68 and then assessed for the snowflake divertor in Ref. 66. It mostly affects poloidally trapped ions with the turning points near the divertor null. In the course of their motion along the field line from the outer midplane to the inner midplane, the ions encounter a growing toroidal magnetic field that scales as $1/R$, with R being a distance to the geometrical axis. As the magnetic moment of the ions is conserved, those of them that have a pitch-angle corresponding to their reflection near the divertor PF null, spend a very long time in the vicinity of the reflection point. This effect occurs in the standard divertor as well but manifests itself much stronger in the snowflake, since the poloidal field is very low here, and poloidal projection of the particle velocity turns virtually zero. Then, for the ion drift velocity directed downward, the ion will escape the confinement zone and eventually hit the divertor target.

In order to be lost by this channel, the ion has to start near the separatrix. The affected zone is larger for the snowflake divertor than for the standard one. Figure 20 shows the characteristic particle trajectories for the snowflake. Depending on their initial starting point and pitch angle, the ions may end up in any of the four strike points. For the green trajectory in Fig. 20, the particle will leave along the leftmost branch of the separatrix, whereas the red trajectory corresponds to the particle lost along the lower right branch. This effect may contribute to the appearance of some heat and particle flux on those branches of the separatrix that are not connected with SOL, when the configuration is near an exact snowflake.

A more quantitative analysis is based on the drift equation of motion for the ions near the poloidal field null. The parallel ion velocity is determined by the conservation of the ion energy W and magnetic moment. We consider the ions moving near the separatrix and are interested in the ions whose parallel motion has a turning point not far from the

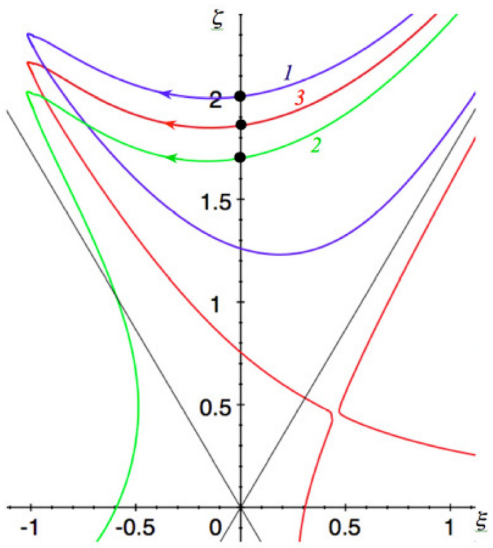

FIG. 20. Characteristic particle trajectories for the ions with the turning points near the snowflake null. Reprinted with permission from Phys. Plasmas **17**, 014501 (2010). Copyright 2010 AIP Publishing LLC.

null-point. Denoting the x-coordinate of the turning point by x^*, one can write the following expression for the parallel velocity in terms of the particle energy W:

$$v_{\parallel} = \mp\sqrt{\frac{2W}{m_i}}\sqrt{\frac{x-x^*}{R}}, \tag{57}$$

where we assume that $x^* \ll R$. The sign "minus" ("plus") corresponds to the particle moving to the left (to the right). We assume that the ion gyroradius is small compared to other spatial scales and use zero gyro-radius drift approximation.

The ion drift is determined by the curvature and gradB drifts (for now we neglect the possible presence of the electric field). The analysis is significantly simplified by the fact that the ion parallel velocity not far from the turning point is much smaller than the ion perpendicular velocity. This allows us to neglect the curvature drift compared to the *gradB* drift, thereby yielding very simple equations of motion

$$\dot{x} = -\frac{v_{\parallel}}{B_T R}\frac{\partial \Phi}{\partial y}; \quad \dot{y} = \frac{v_{\parallel}}{B_T R}\frac{\partial \Phi}{\partial x} - \frac{c}{e}\frac{W}{RB_T}. \tag{58}$$

This system can be reduced to the following full differential form:

$$\left(\frac{\partial \Phi}{\partial y}dy + \frac{\partial \Phi}{\partial x}dx\right) = d\Phi = \frac{c}{ev_{\parallel}}Wdx. \tag{59}$$

Using Eq. (57), one can integrate Eq. (59) to produce the ion trajectory,

$$\Phi(x,y) \pm \frac{c\sqrt{2m_i W}}{e}\sqrt{\frac{x-x^*}{R}} = const. \tag{60}$$

Note that in this derivation we have not made any specific assumptions regarding the flux function Φ. In other words, Eq. (60) is applicable both for the snowflake and standard geometry. For the electrons, this mechanism is inefficient:

due to their small mass, the second term in l.h.s. of Eq. (60) can be neglected, signifying that the electrons follow the flux surfaces.

In the case of an exact snowflake, with Φ defined by Eq. (25), the characteristic spatial scale of the zone affected by the prompt loss is

$$\Delta_{SF}^{(prompt)} \sim a\left(\frac{\varepsilon}{K_2}\right)^{2/5}, \tag{61}$$

with

$$\varepsilon \equiv \frac{c\sqrt{2m_i W_i}}{aB_{PM}e}\sqrt{\frac{a}{R}}. \tag{62}$$

By the order of magnitude, ε is a poloidal ion gyroradius in the midplane, divided by a and multiplied by the square root of the inverse aspect ratio. Typical value for ε in the existing tokamaks for the W_i identified with the ion temperature $\sim$100 eV is $\sim$0.01, so that $\Delta_{SF}^{(prompt)}/a \sim (0.1-0.12)a$. When projected to the outer midplane, the width of the affected zone is $\sim(\Delta_{SF}^{(prompt)})^3/a^2 \sim a\varepsilon^{6/5}$, i.e., on the order of 1–2 mm.

For the standard divertor described by Eqs. (9) and (10), one finds

$$\Delta_{SD}^{(prompt)} \sim a\left(\frac{\varepsilon}{K_1}\right)^{2/3}. \tag{63}$$

The affected layer is much narrower than for the snowflake, both near the null and when projected to the midplane.

In the previous discussion around Equation (61), we considered the model where the magnetic field is exactly the field of a snowflake. This model remains valid if the distance between the nulls is smaller than the size of the affected area determined by Eq. (61),

$$D < \Delta_{SF}^{(prompt)}. \tag{64}$$

This is a condition where the prompt losses "do not notice" the difference between the snowflake and quasi-snowflake.

Consider now the prompt loss under condition where the distance D is greater than that defined by Eq. (64). Until D is small compared to the minor radius, a quasi-snowflake description of the magnetic field, Eq. (10), will be valid, but the field near the main null will now depend linearly on the distance; i.e., in order to evaluate the affected zone, one has to use Eq. (63). However, instead of the order-one coefficient K_1, one would have to use a coefficient $K_2 D/a \ll 1$. Equation (63) then shows that the zone of the prompt loss will be affected by the presence of the second null and will have a size

$$\Delta^{(prompt)} \sim a\left(\frac{\varepsilon a}{K_2 D}\right)^{2/3}. \tag{65}$$

For $D \sim \Delta_{SF}^{(prompt)}$, Eq. (65) would yield the same value for the affected zone as Eq. (61). For increasing D, the size of the effected zone will decrease and eventually, at $D \sim a$, will become the same as for the standard divertor, Eq. (63). This example shows that the "conversation" between the two nulls continues until their separation becomes of order a.

Another geometrical aspect of the problem is the tilt of the whole configuration with respect to the vertical axis. In our analysis, we assumed that the asymptotes of the main separatrix are symmetric with respect to the device geometric axis. For real devices, this may not be the case and, although a qualitative estimates will remain the same, specifics of the trajectories and the distribution of the lost ions between the strike points may change. This interesting problem may help in the experimental identification of the prompt losses. These effects have not been studied experimentally but may potentially play a significant role in defining a structure of both pedestal and SOL.

The same basic effect modifies the neoclassical trajectories even of those ions in the vicinity of the separatrix that do not experience prompt loss. There exist a host of yet to be solved theory problems regarding potential effect on the transport near the separatrix and the SOL structure, especially if the models of the type proposed in Ref. 100 are applicable.

In terms of the energy sink by prompt ion loss, this is a small effect, because these ions occupy a small part of the velocity space, the part corresponding to the location of the turning points near the divertor null, i.e., to a narrow range of equatorial pitch angles. On the other hand, this ion loss channel is expressly nonquasineutral. Obviously, the quasineutrality will be maintained by formation of the electric field that would keep the ion and electron losses equal—a concept already discussed in the context of the standard divertor (Refs. 67 and 68). A complete study of this problem is a task for the future work. The electric field, in turn, will determine the velocity shear in the pedestal and thereby may affect the stability of the pedestal. This observation brings us naturally to Section VII, where experimental results related to the effect of the snowflake geometry on the pedestal and core are summarised.

VII. IMPACT OF SECOND NULL ON CORE AND PEDESTAL

The superposition of several conjectured effects discussed in Sec. II–IV can create a pretty complex pedestal picture, with a subtle interplay of magnetic shear, velocity shear, and edge neoclassical effects.

The presence of the second poloidal field null in the vicinity of the separatrix leads to the increased edge flux-surface-averaged safety factor q and magnetic shear. Increased magnetic shear inside the separatrix can in turn affect the edge turbulence and H-mode confinement. For example, in conventional and spherical tokamaks, the L–H power threshold is significantly lower in a double null configuration (where the second upper X-point is on the same flux surface as the lower one). The higher flux-surface-averaged magnetic shear just inside the separatrix predicted for the SF configuration can also lead to stronger stabilization of ideal current-driven peeling modes and pressure-driven ballooning MHD modes. A noticeable increase of the ideal stability threshold was found in Refs. 59 and 60 (see more detail below, Fig. 21). However, a computational study[61] of a

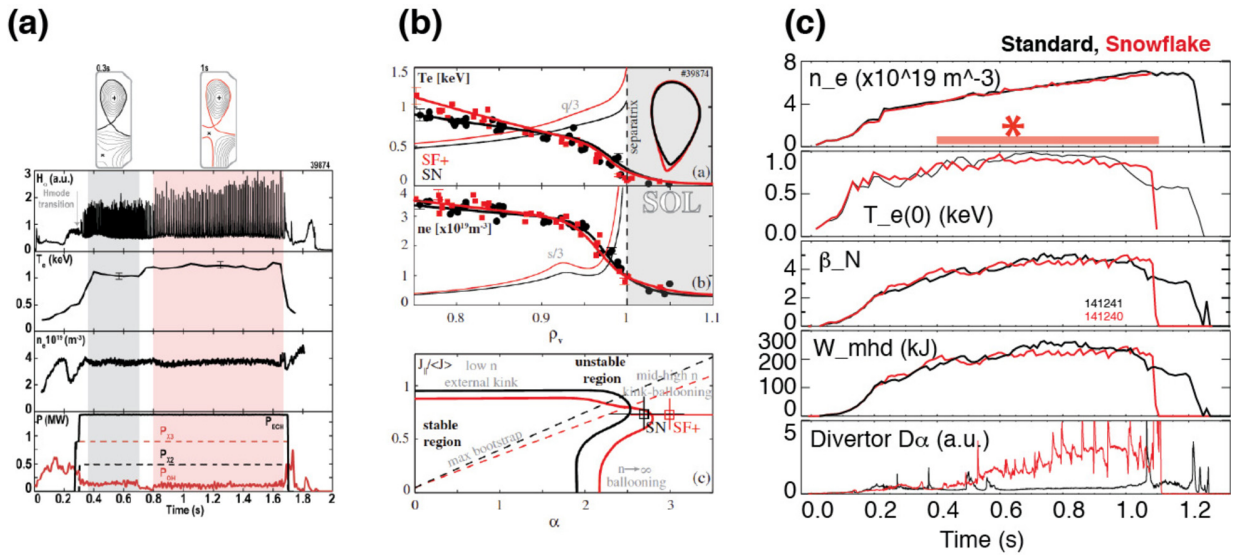

FIG. 21. Effect of snowflake divertor configurations on core and pedestal plasmas and ELMs in TCV and NSTX. (a) TCV time traces (Cf. F Piras, Ref. 101): H_α edge emission; volume averaged electron plasma temperature; line averaged electron plasma density; Ohmic power (red solid line), ECH-X2 power (black dashed line), ECH-X3 power (red dashed line), and total ECH power (black solid line). (b) TCV radial plasma profiles (top two panels): Electron temperature and density pedestal profiles for the standard and snowflake. configurations (solid lines) together with the Thomson scattering measurements (dots). Thin lines represent the q = 3 profile (top panel) and the magnetic shear s = 3 (middle panel). Stability diagrams (bottom panel) of the standard and snowflake configurations. The collisional bootstrap current is represented by dashed lines together with the experimental points for both configurations (squares). Courtesy F. Piras. Reprinted with permission from Phys. Rev. Lett. **105**, 155003 (2010). Copyright 2010 American Physical Society. (c) NSTX time traces of core and edge plasma quantities in the standard divertor (black traces) and snowflake (red) configurations: Averaged density n_e; Central electron temperature T_e; Normalized βN; Core plasma stored energy W_{tot}; and lower divertor total D_α intensity. Reprinted with permission from Phys. Plasmas **19**, 082504 (2014). Copyright 2012 AIP Publishing LLC.

linear peeling-ballooning mode stability in the standard and snowflake-plus divertor configurations showed that the effect on stability was opposite (albeit weak). An explanation suggested in Ref. 61 was related to the mode structure in the standard divertor: the drive and the mode were localized near the outer mid-plane, and the shear in the mid-plane area was sufficiently strong to completely damp the mode on the way to the null. As the mode in the vicinity of the null was essentially absent, introducing a stronger shear near the null had only minor effect on the mode. On the other hand, some changes of the overall configuration between two cases gave rise to a weaker stability of the snowflake, i.e., the mid-plane magnetic shear was important. One can also phrase this conclusion in a somewhat different way: while the high-n peeling-ballooning mode growth rate was suppressed in the null-region of the snowflake divertor (cf. standard divertor), it was higher in the mid-plane where local magnetic shear was actually lower.

In the experiment, pedestal modification due to the snowflake configuration was observed in the TCV, NSTX, and DIII-D, as discussed below. Although details varied, there was also quite robust common feature in all three devices: unaffected stored plasma energy and core confinement.

In TCV,[101,102] H-mode threshold was systematically studied by varying the ECH power in the range of 0.25–1.5 MW in otherwise similar discharges having the standard divertor and snowflake-plus configurations. The L–H transition threshold was found to be similar in both cases over the density range $3–7 \times 10^{19}$ m^{-3}. Modest confinement improvement, up to 15%, was observed in the snowflake-plus phase, however, possibly also due to increased core shaping. The snowflake-plus configuration in TCV had a profound effect on the pedestal stability. The frequency of Type I ELMs decreased by 50%–80% at the transition from the standard divertor to the snowflake configuration, while the energy loss per ELM increased only by 20%–30%, apparently consistent with Ref. 60. The snowflake-plus phase of the H-mode discharge therefore indicated improved performance with reduced energy lost through the ELM channel. Pedestal MHD stability calculations indicated that the stability operating point in both the standard divertor and the snowflake-plus was close to the kink-ballooning stability boundary, and the snowflake-plus configuration was consistent with improved kink-ballooning stability.[60,101] Additional calculations of stability sensitivity to variations in pedestal pressure gradient and edge shaping revealed that the edge stability of the snowflake configurations is enhanced. However, the shaping (increased triangularity) also contributes to the enhanced stability of the edge kink-ballooning modes. In these studies, free boundary snowflake equilibria and experiment-like pedestal pressure profiles were used.[60]

In NSTX,[52,79] core plasma parameters (e.g., n_e, central $T_e \sim 1$ keV, $\beta_N \sim 4.5$) were similar in the standard and snowflake divertor H-mode discharges. Similar high performance metrics of these discharges, e.g., $\tau_E \sim 50–60$ ms, $W_{MHD} \sim 200–250$ kJ (the total plasma stored energy as evaluated by EFIT magnetic reconstruction code), and the H-mode confinement enhancement factor H98(y,2) ~ 1 calculated using the TRANSP code, were inferred in both divertor configurations. The snowflake divertor phase had a profound effect on plasma impurity content: the total carbon inventory was reduced by 50%–70%. The observed reduction was attributed to the reduction of carbon physical sputtering

fluxes in the partially detached snowflake divertor (due to very low divertor T_e), and to the particle expulsion effect from ELMs that reappeared in the snowflake phase. The transition to the snowflake configuration led to a clear and reproducible destabilization of the ELMs. These large ELMs were classified as Type I, with somewhat irregular frequency of $f = 12–35$ Hz and $\Delta W_{MHD}/W_{MHD}$ in the range of 5%–10%.

In DIII-D,[76] both the magnetic shear and q_{95} were systematically increased by 10%–30% in the snowflake configuration. Edge plasma profiles were similar with and without the snowflake. Pedestal top plasma parameters varied within 5%–15%: with the snowflake configuration, T_e^{ped} slightly reduced, n_e^{ped} slightly increased, and p_e^{ped} remained nearly constant. Changes in the magnetic shear and weak changes in pedestal pressure gradient were apparently insufficient to significantly affect the peeling-ballooning mode stability, as only small increases in ELM frequency ($\leq$10%–20%) were detected. The pedestal energy W_{ped} was nearly unaffected at lower n_e. The pedestal stored energy loss per ELM ΔW_{ELM} was reduced in discharges with the snowflake configurations. In some discharges, the effect was strong and ΔW_{ELM} was reduced by up to 50%. More typically, however, the reduction was in the range of ~10%–20%.

VIII. RADIATIVE SNOWFLAKE DIVERTOR

Future divertor power exhaust solutions are likely to involve radiative detachment for increased volumetric power and momentum losses and reduced material erosion. From the divertor geometry arguments, the snowflake divertor has the potential to increase divertor radiated power losses via longer connection length that leads to lower divertor T_e and greater flux tube volume, and larger divertor physical volume due to the expanded flux tubes. Transport and drift effects, e.g., increased radial transport and modification in the parallel impurity transport, can also play a role. The tokamak snowflake experiments used D_2 and impurity seeding in initial studies of impurity radiation distribution and detachment in the snowflake divertor.

In NSTX,[52,79] a remarkable effect was observed even in the absence of additional gas seeding: the snowflake-minus configuration led to the onset of partial detachment, otherwise inaccessible at the same upstream parameters in the standard divertor configuration. The partial detachment was characterized by the loss of electron pressure along the flux tube (estimated as n_eT_e from the measurements upstream and in the divertor), increased carbon radiated power, and a significant increase of volumetric recombination. The divertor peak heat flux was also reduced by up to 80%. This was thought to be a combined effect of the flux expansion on deposited heat flux, the increased power loss in the radiative divertor, and possible sharing of power between all snowflake strike points.

In DIII-D, radiative snowflake experiments were performed in two settings.

Experiments performed in lower snowflake-minus or -plus configurations with D_2 seeding[76] showed that (cf. standard divertor), Fig. 22: (1), both the radiative snowflake-minus and snowflake-plus were compatible with the H-mode albeit with

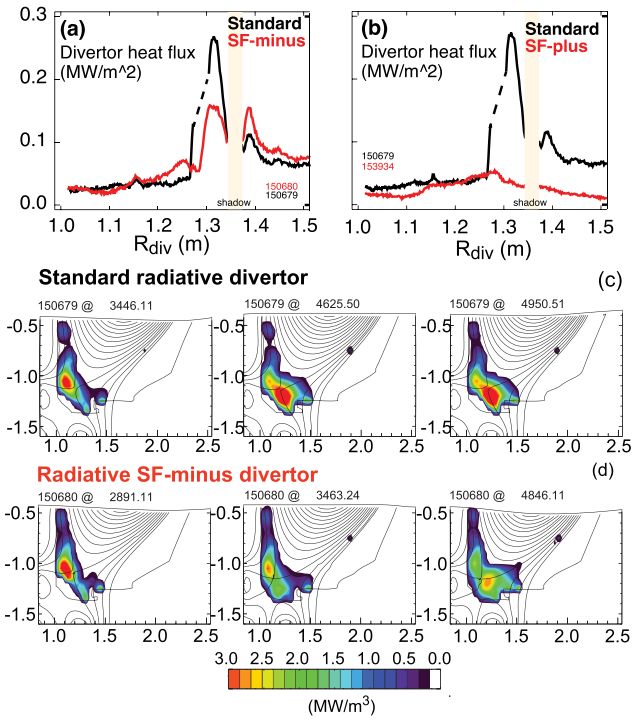

FIG. 22. Inter-ELM divertor heat flux profiles in the radiative divertors in DIII-D in the standard, snowflake-minus (a), and snowflake-plus (b) configurations. Radiated power density distribution during a transition to the radiative divertor in the standard (c) and snowflake-minus configurations (d). Reprinted with permission from Soukhanovskii *et al.*, J. Nucl. Mater. **463**, 1191 (2014). Copyright 2014 Elsevier.

confinement degradation with respect to a standard radiative divertor H-mode discharge with a similar (within 10%) core density; (2) the reduction of inter-ELM divertor heat fluxes was stronger in the snowflake configurations, leading to nearly complete power detachment at $P_{SOL} \sim 3–4$ MW (Fig. 22); (3) carbon and deuterium emissions were more broadly distributed in the snowflake configurations, including the additional divertor legs, at divertor radiation fraction $f_{rad} \sim 0.5–0.7 \times P_{SOL}$ and otherwise similar edge and core parameters.

Experiments were also performed in a configuration with the upper single null and lower snowflake-minus with B-grad B directed toward the upper divertor and neon and D_2 seeding[103] in an attempt to combine the radiative snowflake configuration with a high-performance advanced tokamak H-mode scenario. While the peak heat flux reduction was about 50% stronger in the radiative snowflake than in the standard radiative divertor with comparable core confinement (e.g., $H98(y,2) \sim 1.30$, $\beta_N \sim 2.9$), neon accumulation was 30%–40% higher in the radiative snowflake case. As cryopumping was used for neon inventory control, the need for better understanding of compatibility of cryopumping with high-flux expansion was concluded.

Neon seeding was used in TCV ohmic experiments to study radiated power distribution in the standard and snowflake-plus configurations.[104] A modest increase in divertor radiation was observed in the snowflake. The radiated fraction of the exhaust power was limited by the onset of a long-wavelength MHD instability making it difficult to compare threshold density of the divertor leg detachment onset and

radiative limits of the snowflake. Studies with D_2 seeding demonstrated the opposite effect: total radiated power was systematically slightly higher in the standard divertor configuration.

IX. SNOWFLAKES FOR FUTURE FACILITIES

A. Poloidal field coils

In future reactor-scale tokamaks, it is highly desirable to place the PF coils outside the toroidal field (TF) coils. This requirement sets the limit on how close can the PF coils be placed with respect to the divertor. Due to larger distances to the coils, the coil current required to create the magnetic field sufficient to neutralize the field of the plasma current at a given point inside the vessel becomes significant, thereby imposing constraints on the coil design. Both current-carrying capability and mechanical forces acting on the coils have to be considered. This problem has been studied for the standard divertor for ITER-scale devices, with a favourable conclusion,[82] but it has to be re-assessed for the divertors using more complex field structures, like a snowflake.

For the snowflake divertors, the problem of PF coil system in reactor-scale facilities has been addressed in Refs. 72 and 105, also with a favourable conclusion. General procedures for optimizing the coil positions for a desired plasma shape have been discussed in Ref. 72. The main point here is that one has to use the number of coils comparable to that of ITER or by a few more and, more importantly, optimize both the placement of the coils and current distribution between them.[72] By increasing the number of poloidal field coils and optimizing their positions, a significant performance improvement in terms of the current-carrying capacity has been reached. This optimisation procedure has proven its efficiency when applied to the existing devices: in Ref. 83, the optimization of the current distribution in the existing coil set in the TCV tokamak has led to the possibility to operate at the plasma current 20% higher than for the unoptimized currents.

Fig. 23(a) shows the coil system developed for the DEMO reactor,[72] and Fig. 23(b) shows a coil system developed for CFETR; a clearly recognizable SF+ magnetic field structure is visible. Feasibility of a quasi-snowflakes on a superconducting tokamak EAST was demonstrated in Ref. 81, albeit at a relatively low plasma current. More work is needed to assess the limitations set by the mechanical forces on the coils.

Most challenging is creation of the double-null (up-down symmetric) snowflake.[106] Two divertors use up a significant fraction of the volume inside the TF coils. In addition, the field of a lower set of the divertor coils adds to the plasma field in the location of the upper null and thereby forces one to increase the current in the upper set of the coils (and vice versa), leading to the need of excessively high currents in the PF coils.

In a recent study of a super-X divertor for reactor-scale facilities,[107] a couple of PF coils were placed inside TF coils (but outside the shield), to get a better control of the field structure. Properly modified, this approach could possibly be used also to create a SF configuration.

The available designs of the divertor hardware[108] rely on the use of only two "upper" divertor legs, thus making the overall shape of the divertor hardware somewhat similar to that used in the standard divertor. The features of the snowflake used in this design include the stronger flux flaring and higher connection length (cf. Ref. 58). The general conclusion of numerical simulations of these configurations mentioned at the end of Sec. IV A is that the heat load can be reduced by a factor of 2–3 compared to the standard divertor.

Snowflake configuration can potentially be produced in the divertor section of a proposed facility ADX,[74] where a large number of divertor coils provide great flexibility in studying various divertor configurations. The snowflake may be of some interest as it would produce a large quasi-isotropic flux expansion in the divertor chamber.

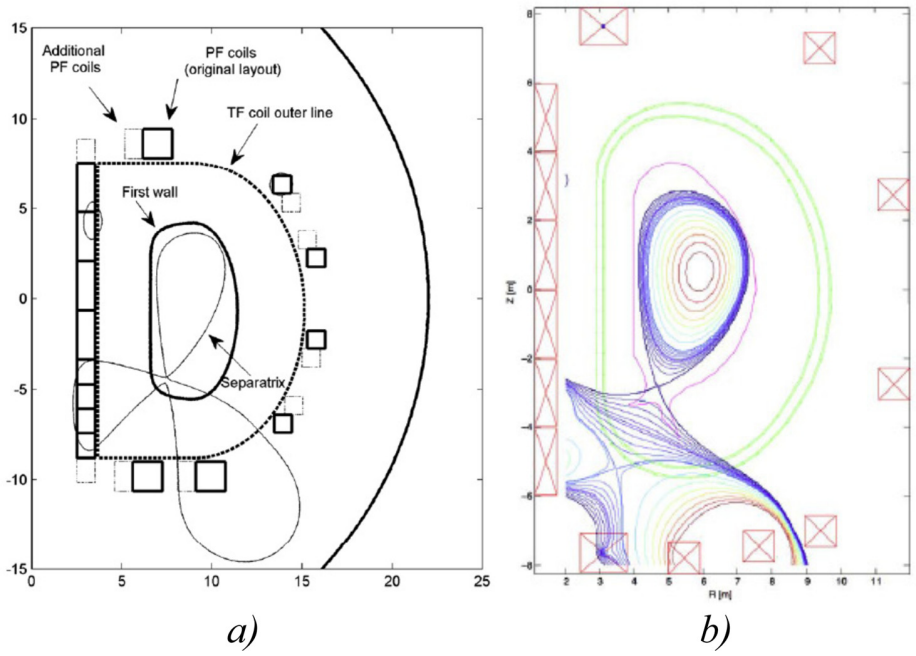

FIG. 23. Poloidal field coil structure for future fusion facilities: (a) A DEMO reactor coil structure for a 15-coil PF system; the lightly marked coils are in non-optimum positions used as a first iteration, whereas bright squares show the final positions. Courtesy R. Albanese *et al.*[72] Reproduced with permission from Albanese *et al.*, Plasma Phys. Controlled Fusion **56**, 035008 (2014). Copyright IOP Publishing. (b) CFETR experimental reactor. This divertor structure utilizes two upper divertor legs of a SF+ configuration. Courtesy Z. Luo *et al.* Reprinted with permission from Luo *et al.*, IEEE Trans. Plasma Sci. **42**, 1021 (2014). Copyright 2014 IEEE, Ref. 105.

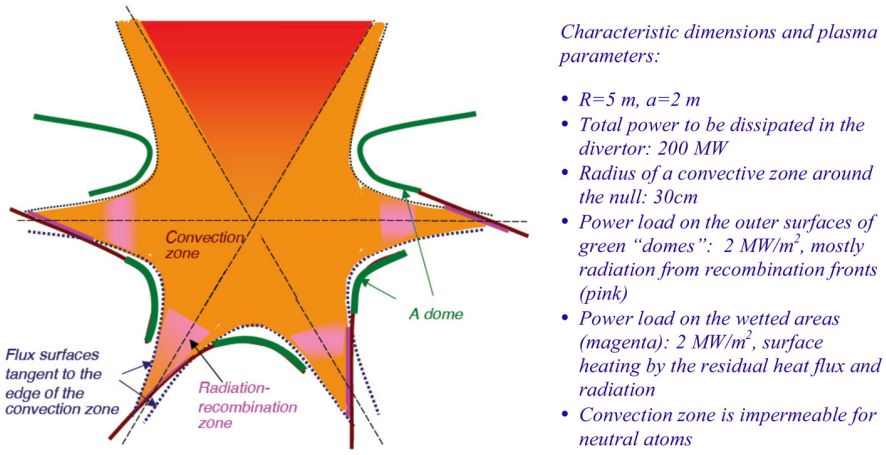

FIG. 24. A cartoon illustrating a concept of a radiative SF divertor for fusion reactors. The area between the target and radiative-recobination zone is filled with a weakly ionized plasma.

B. Radiatively detached snowflakes for reactors?

There are no comprehensive design studies of the possible structure of the snowflake divertors utilizing flux sharing between all divertor legs. If further experiments demonstrate scalability of this effect to larger, reactor-scale devices, then one could attempt to utilize it in the divertor design. A possible approach was suggested in Ref. 109 and is briefly outlined below. We emphasize that the whole concept is still hypothetical, not supported by detailed numerical simulations or dedicated experiments. Still, as it may eventually lead to breakthroughs in the divertor development, we take a risk to discuss it below. The numerical values of the plasma parameters provided below are notional.

The overall divertor structure is shown in a cartoon form in Fig. 24. The zone around the null is filled with a plasma appearing there via one of the anomalous transport mechanisms mentioned in Sec. V. To be specific, we assume that this mechanism is a convective transport (cf. Fig. 17(b) above). Inside the convective zone, the temperature and density are similar to those at the last-closed flux surface. We assume the values of $T_e = 50-100\,\mathrm{eV}$ and $n_e = (1-3)10^{13}\,\mathrm{cm}^{-3}$. For the size of the zone of 30 cm, it would be impermeable to the neutrals born at the interface of this zone with a colder divertor plasma (cf. Ref. 11 for the atomic cross-sections). In other words, the core plasma is shielded from the influx of neutrals from the divertor region, this protecting it from an uncontrolled density growth in the null-point region.

The outer boundary of the convection zone is determined by the rapid growth of the poloidal magnetic field at some distance from the null. The convection ceases to exist there, and the plasma continues its flow away from the convection zone along the four divertor channels in a regular way similar to that of the standard divertor. The most plausible location of the radiation-recombination zone is in the area of this transition, where the plasma temperature has already dropped. The front cannot expand towards the null because of the aforementioned impermeability of the convection zone to the neutrals.

One can expect that the plasma is fully detached from the divertor targets, due to a very large wetted area and associated heat flux reduction: the plasma flow to the divertor legs is significantly widened by the plasma convection, and there are four active strike points. On the other hand, as mentioned, the neutrals are shielded from the core plasma by the plasma of the convective zone (not by convergence of the magnetic flux, as discussed in Ref. 110). Clearly, this discussion is not based on a consistent quantitative analysis and is therefore hypothetical. Still, it identifies interesting possibilities and may lead to development of more comprehensive models.

The targets are situated in the area of a significantly re-compressed poloidal field, where the field structure looks like that of the "perfect" snowflake. The targets are tilted with respect to the poloidal field vector (by $\sim 30^\circ$ for the structure shown in Fig. 24). The tilt here is limited by the same engineering constraints as in the standard divertor: the angle of the total field vector cannot be too shallow with respect to the target surface. Large volumes available for the neutral handling are protected by the domes (green structures in Fig. 24); the outer surfaces of the domes receive radiation flux from the convective zones as well as from recombination zones.

The presence of the convective zone leads to smoothing of the plasma pressure profile in the pedestal region. This may be a favourable factor in controlling the ELMs. Note that in the experiments where a power sharing between the divertor legs was observed (Secs. IV and V), it was not accompanied by any significant confinement degradation. Note that there is no need to have an "exact" snowflake for this concept to work: what is necessary is that the distance between the two nulls be smaller than the size of the convection zone; for the radius of the convection zone $D \sim 0.1a$ (Eq. (56) for $\beta_{pm} \sim 1/200$), this is a task that seems to be manageable, given that the values of $D/a \sim 0.1$ have been routinely created on the existing experimental facilities.

Note that the convection driven by the pressure gradient is just one of several mechanisms that may lead to the heat flux spreading near the divertor null. Other effects may also lead to the same outcome: the E × B convection, the ballooning modes, and magnetic field stochastization in the area of the low poloidal field; these effects may have different from Eq. (56) scaling.

Assuming that the divertor has to handle a power of 200 MW, and for the other parameters as indicated in Fig. 24, one can create the situation where the heat flux on the material surfaces of the domes and target plates will not exceed a few MW/m^2. This design allows deploying several targets in the same divertor volume, thereby leading to a much more compact divertor. Again, at present, this is still a hypothesis.

C. SF divertor in the absence of convective heat flux sharing

If the plasma or field parameters are such that there is no significant convection near the main null, one can still exploit the features of the snowflake divertor to generate more than two strike points, as mentioned in Ref. 36 and discussed in Sec. IV. To do that, one has to create a snowflake-minus configuration with the second null lying within the scrape-off layer, Then, the flux in the outer SOL will be split between two divertor legs, thereby leading to the formation of an extra strike point. The first consistent analysis of this possibility has been recently made by Lunt *et al.*[86] who have used EMC3-Eirene code to assess a complex field structure of this configuration. They have found that significant improvement with respect to the standard divertor is possible for similar plasmas. One can speculate that additional, even modest, convective spreading caused by a low value of $d|B_p|/dr$ near the main null may lead to quite an attractive design (for TCV, some increased transport is observed for the parameter σ, Eq. (42), of order 0.2, Ref. 75).

D. Other two-null divertors

There is a special two-null configuration[36] that was called "a tripod" in Ref. 73, Figs. 5(f) and 5(k) of our paper. If the distance D between these two nulls is small, then the effect of this configuration on the scrape-off layer and plasma convection would be indistinguishable from those of an exact snowflake. Consider, however, the situation where D exceeds the distance for which these effects take place (Secs. III B and V) but still satisfies a condition $D \ll a$. For such distances, the two tripod nulls *do* affect each other in that the field flatness in both nulls is the same and scales linearly with D. For $D < a$, derivatives $d|B_p|/dr$ in both nulls are smaller than a "natural" value for an isolated first-order null. This circumstance can be used in the arrangement leading to Pitts' divertor[30] or X-point target divertor.[74]

X. SUMMARY

The snowflake divertor is based on the magnetic configuration with two nearby first-order nulls that appear if the field possesses certain smoothness properties. When the nulls merge, one gets a single second-order null that generates a separatrix with six "rays" going out from the null and reminiscent, symmetry-wise, of a snowflake. When the second-order null splits into two nearby nulls, the asymptotes to the separatrix still maintain this six-fold symmetry.

Since the first publications on the snowflake divertor,[34–36] the analyses of the divertor field were made for the practically important case of the divertor coils situated far away from the divertor. In this case, the aforementioned field smoothness appears automatically. The flux function and the poloidal field in the divertor zones are then universal smooth functions of coordinates and can be presented as simple polynomial expansions (two-null representation). The presence of this expansion is a consequence of the underlying properties of the smooth magnetic field. Remarkably, one can control a broad variety of these two-null configurations by changing currents in the remote coils—this provides significant flexibility in selecting a configuration best suitable for a particular device.

The physics of the snowflake divertor is strongly affected by the "conversation" between the two nulls that shows up, in particular, in the effect of one null on the magnetic field "flatness" at the other null and on the overall shape of the separatrices. The "flatness" characterizes the flux expansion near each null, whereas the overall shape determines the way by which magnetic structure interacts with the core plasma and the divertor targets.

The snowflake divertor has been realized and studied on several tokamaks. A number of interesting effects has been discovered: they are partially described in this article. An important effect that may lead to a very attractive divertor design is the heat flux sharing between multiple strike points.

In addition to being a contender for developing a workable divertor for future fusion facilities, it brings up also a set of interesting physics questions related to our understanding of the plasma transport for complex magnetic topology. A great flexibility of the snowflake-based magnetic configurations controlled by remote coils creates a platform for a deeper understanding of the divertor physics, a "laboratory for the divertor physics."

ACKNOWLEDGMENTS

We acknowledge many years of fruitful collaboration on the snowflake physics with our colleagues from several institutions. We believe that our discussions with them helped us to reach a better understanding of the physics involved. We are particularly grateful to S. Allen, G. P. Canal, R. H. Cohen, W. A. Farmer, S. Kaye, E. Kolemen, J. Menard, M. Ono, H. Reimerdes, T. D. Rognlien, and M. V. Umansky. One of us (V.S.) is indebted to the entire teams of NSTX and DIII-D facilities for their help during the snowflake experimental campaigns. Possible errors or inconsistencies in this paper are entirely the authors' responsibility.

This work was performed under the auspices of the U.S. Department of Energy by Lawrence Livermore National Laboratory under Contract No. DE-AC52-07NA27344. This material is based upon work supported by the U.S. Department of Energy, Office of Science, Office of Fusion Energy Sciences.

APPENDIX A: TOROIDICITY EFFECT IN THE TWO-NULL REPRESENTATION

The analysis of the geometrical features of the snowflake magnetic field in Secs. II and III was based on the approximation of the "planar" field, where the field has x and y components in the Cartesian coordinates x and y

$$B_x = B_x(x,y); \quad B_y = B_y(x,y)\,. \tag{A1}$$

This approximation does not account for the toroidicity effects that enter the problem via the terms of order of x/R_0 and y/R_0, with R_0 being a major radius corresponding to the origin of the Cartesian coordinates.

To address this issue explicitly, we introduce cylindrical coordinates (R, ϑ, y) with R being a distance of an observation point to the geometrical axis. Note that, instead of the standard notation "z" for the axial coordinate, we use notation "y," to avoid confusion with the complex variable z used throughout this paper. We then introduce coordinate x according to: $R = R_0 + x$, so that we can establish a direct correspondence to the notation (x, y) used in the rest of this paper (Fig. 1).

The poloidal field with toroidal symmetry can be presented as a curl of the toroidal component of the vector potential A_ϑ. Instead of A_ϑ, it is more convenient to use a function

$$\Phi = \frac{R}{R_0}A_\vartheta = \left(1 + \frac{x}{R_0}\right)A_\vartheta. \tag{A2}$$

The magnetic field is expressed as

$$B_x = -\frac{1}{1+\dfrac{x}{R_0}}\frac{\partial\Phi}{\partial y}; \quad B_y = \frac{1}{1+\dfrac{x}{R_0}}\frac{\partial\Phi}{\partial x}\,. \tag{A3}$$

The function Φ is a flux function, with the iso-contours $\Phi(x,y) = const$ of this function determining the flux surfaces in the x,y plane. This statement now is not based on the assumption of the zero toroidicity, $1/R \to 0$.

The condition $\nabla \times \boldsymbol{B}_p = 0$ reads as $\partial B_R/\partial y - \partial B_y/\partial R \equiv \partial B_x/\partial y - \partial B_y/\partial x = 0$ (we have used relations $R = R_0 + x$ and $B_R \equiv B_x$); together with Eq. (A3), this yields

$$\frac{\partial^2\Phi}{\partial x^2} + \frac{\partial^2\Phi}{\partial y^2} - \frac{1}{R_0 + x}\frac{\partial\Phi}{\partial x} = 0. \tag{A4}$$

Eqs. (A3) and (A4) become identical to Eqs. (2) and (5) in the limit of a small toroidal curvature.

Consider now corrections to the flux function (and, thereby, to the shape of flux surfaces) caused by the finiteness of $1/R$. We have noticed in Sec. III that, for the distance D between the two nulls of the quasi-snowflakes less than a, the flux function in the limit of $1/R \to 0$ has the following form:

$$\Phi^{(0)} = (B_{pm}K_2/a^2)[P_3(x,y) + D^2P_1(x,y)], \tag{A5}$$

where P_3 and P_1 are polynomials of the third and first power, respectively, with the coefficients of order one and the superscript "0" $\Phi^{(0)}$ meaning that this is a flux function of a zeroth-order in $1/R$. As an example, in the exact snowflake $P_3 = xy^2 - (2/3)y^3$, $P_1 = 0$. To find a correction of order $1/R$, we substitute Eq. (A5) into the last term in Eq. (A4) to find equation for the first-order correction

$$\frac{\partial^2\Phi^{(1)}}{\partial x^2} + \frac{\partial^2\Phi^{(1)}}{\partial y^2} \approx \frac{1}{R_0}\frac{\partial\Phi^{(0)}}{\partial x}\,, \tag{A6}$$

where we dropped the term x/R_0^2 in the r.h.s that would have led to a small higher-order correction. The r.h.s. is obviously a sum of the polynomial of the second order and a constant. In other words, the polynomial solution for $\Phi^{(1)}$ will be a sum of the fourth-order and second-order polynomials, and the general expression for Φ will be

$$\Phi \approx (B_{pm}K_2/a^2)[P_3(x,y) + D^2P_1(x,y) + (1/R_0)(P_4(x,y) + D^2P_2(x,y))]. \tag{A7}$$

One sees that the ratio of the curvature terms to the main ones is of order x/R, $y/R \ll 1$ and does not affect the shape of the flux surfaces in the divertor area, Fig. 5.

APPENDIX B: SENSITIVITY TO THE CORE PLASMA CURRENT VARIATION

The structure of the magnetic field in the divertor area is determined by both the plasma current and current in the poloidal field coils. It is important to evaluate the effect of the varying magnitude and spatial distribution of the plasma current for the case where the PF coil current is held constant. This would allow one, in particular, to find requirements to the plasma control system: how will the magnetic configuration change, if control system does not react on some variation of the plasma current and its centroid.

Assuming that the plasma current and its distribution in the poloidal plane vary by some small amount, and starting from the exact snowflake configuration, $G = K_2B_{pm}z^3e^{i\eta}/3a^2$, one can account for the small changes of the plasma current by adding perturbations to the flux function

$$G = \frac{K_2B_{pm}e^{i\eta}}{3a^2}z^3 + \alpha z, \tag{B1}$$

where α is a small (generally speaking, complex) parameter proportional to the perturbation. We ignore the contribution of the second and higher order in z, as for small z they will obviously produce much weaker effect than the retained first-order term. The parameter α contains both the contribution of the total current variation and the current spatial redistribution. The contribution to α from the current variation is $\sim(\delta I/I_0)B_{pm}$. Assuming that the contribution of the changing plasma position and plasma shape is of the same order, we then have: $\alpha = QB_{pm}\delta I/I$, where Q is a complex constant of order one that encapsulates both sources of variation, the magnitude of the current and its position. The field function F is

$$F = -\frac{dG}{dz} = -\frac{B_{pm}K_2e^{i\eta}}{a^2}\left(z^2 + \frac{Qa^2e^{-i\eta}}{K_2}\frac{\delta I}{I}\right). \tag{B2}$$

The field now has two null-points,

$$F = -\frac{B_{pm}K_2e^{i\eta}}{a^2}(z - \delta z)(z + \delta z), \tag{B3}$$

with the distance between them

$$\frac{D}{a} = 2|\delta z| = 2\sqrt{\frac{|Q|}{K_2}}\sqrt{\frac{\delta I}{I}} \sim \sqrt{\frac{\delta I}{I}}. \tag{B4}$$

In other words, the uncontrolled current variations lead to establishing some "natural" minimum distance between the nulls. The square root dependence (B4) identified in first snowflake publications[34,35] defines the requirements to the control system that would have to be able to respond to a few per cent of the current variations in order to keep D/a in the range of 0.1. We do not dwell on the straightforward extension of this analysis to the case where the unperturbed state has two deliberately created nulls (a quasi-snowflake).

APPENDIX C: EFFECT OF THE FINITE TOROIDAL CURRENT IN THE DIVERTOR AREA

As the poloidal magnetic field is small in a large area surrounding the snowflake null, one should evaluate the sensitivity of the field structure to possible small deviation of the equilibrium field produced by the presence of a toroidal plasma current in the divertor area: in the analysis of Secs. II and III, we used a curl-free model of the poloidal field.

As the current near the null, especially that on the open flux surfaces, is hard to predict/evaluate, we take an "empirical" approach where we assume some simple model for the current spatial distribution and then find the field structure for various amplitudes of this current.[36,111] As a result, we find a rough estimate of the current that leads to a significant change of the field topology. Having done that, we can make a judgement whether the current of such a magnitude is plausible, or not.

In the vicinity of the null, one can use a planar model, with axial (toroidal) current present. We take the following model for the spatial distribution of that current:

$$j_{div} = \frac{j_{div}^{(0)} D_c^4}{\left[(x-d_{xc})^2 + (y-d_{yc})^2 + D_c^2\right]^2}, \qquad \text{(C1)}$$

where subscript "div" indicates a divertor region. Subscript "c" designates the parameters characterizing the current distribution in the divertor area: the position of centroid (d_{xc}, d_{yc}) and the width of the distribution D_c. For this distribution, the total toroidal current in the divertor area is $I_{div} = \pi j_{div}^{(0)} D_c^2$. We assume that direction of the divertor current is the same as that of the plasma current.

Obviously, the effect on the configuration will be strongest when the current-free configuration is an exact snowflake, where an exact second-order null is most "fragile." Adding the flux function corresponding to the current (C1) to the initial currentless flux function (25), we find an equation for the flux surfaces:

$$-y^3 + 3x^2 y + \mu \ln[(x-d_{xc})^2 + (y-d_{yc})^2 + D_c^2] = const. \qquad \text{(C2)}$$

Here, x, y, and all other parameters of the dimension of length are normalized to the minor radius a, and μ is a dimensionless parameter that characterizes the divertor current density

$$\mu = \frac{3D_c^2}{2K_2 a^2} \frac{j_{div}^{(0)}}{\bar{j}}, \qquad \text{(C3)}$$

where $\bar{j}$ is defined as $\bar{j} \equiv cB_{pm}/2\pi a$ and is approximately equal to the average toroidal current density. In the further discussion, we specified the divertor current density as 0.1 of the average current density. With that, and taking $K_2 = 1$ we show several characteristic shapes of the separatrices in Fig. 25. The parameters that we vary are the position of the centroid and the width D_c of the area occupied by the current. The unperturbed snowflake is oriented so that the bisector of the main separatrix is vertical. In a symmetric case, if the centre of the current flow lies on the bisector, the separatrix acquires a shape close to the symmetric snowflake-minus (panels (a)–(c) in Fig. 25). If the centroid is shifted to the left, towards the axis of the device, one obtains asymmetric snowflakes with the null-to-null distance increasing with the size of the current-carrying area (panels (d)–(f) in Fig. 25). The same happens when the centroid is shifted in the outward direction, just the nulls change places (panels (g)–(i) in Fig. 25). In an improbable case that the current centroid is situated below the unperturbed null, a snowflake-plus configurations are formed (not shown).

An overall conclusion that one can make is that even at significant divertor current density the resulting structures look very similar to vacuum quasi-snowflakes and the general characterization of the plasma effects of the quasi-snowflakes remains unchanged. These results are supported by earlier studies[36,111] of the effect of the divertor currents, where different initial configurations and current distributions were considered.

APPENDIX D: AN HIERARCHY OF CONFIGURATIONS

In this Appendix, we describe a transition from the first-order field null, to the second-order and higher-order nulls in terms of constraints imposed on the field function F, Sec. II. Within the divertor area, F can be represented as a series

$$F = A_0 + A_1 z + A_2 z^2 + A_3 z^3 + A_4 z^4 + \cdots. \qquad \text{(D1)}$$

The corresponding complex potential G (Eq. (8)) will be

$$G = -\left(A_0 z + \frac{A_1}{2} z^2 + \frac{A_2}{3} z^3 + \frac{A_3}{4} z^4 + \frac{A_4}{5} z^5 + \cdots\right). \qquad \text{(D2)}$$

The coefficients A_n depend on the currents in a plasma and PF coils.

For now, we will place the origin at the field null lying on the main separatrix, meaning that $A_0 = 0$. As the scale of the global field variation is $\sim a$,

$$A_n = B_{pm} \frac{K_n e^{i\eta_n}}{a^n}, \qquad \text{(D3)}$$

where B_{pm} is a poloidal field at the midplane and K_n are dimensionless coefficients (real and positive). If no special measures related to the adjustments of the currents are taken (see below), the coefficients K_n are of order one.

For the "standard" first-order null with $K_1 \sim 1$ in the vicinity of the null, i.e., at $|z| \sim D \ll a$, one can neglect the higher-order terms and obtain Eqs. (9) and (11), the second of which we repeat here for convenience

$$G = -A_1 z^2/2 = -K_1 (B_{pm}/a) e^{i\eta} z^2/2. \qquad \text{(D4)}$$

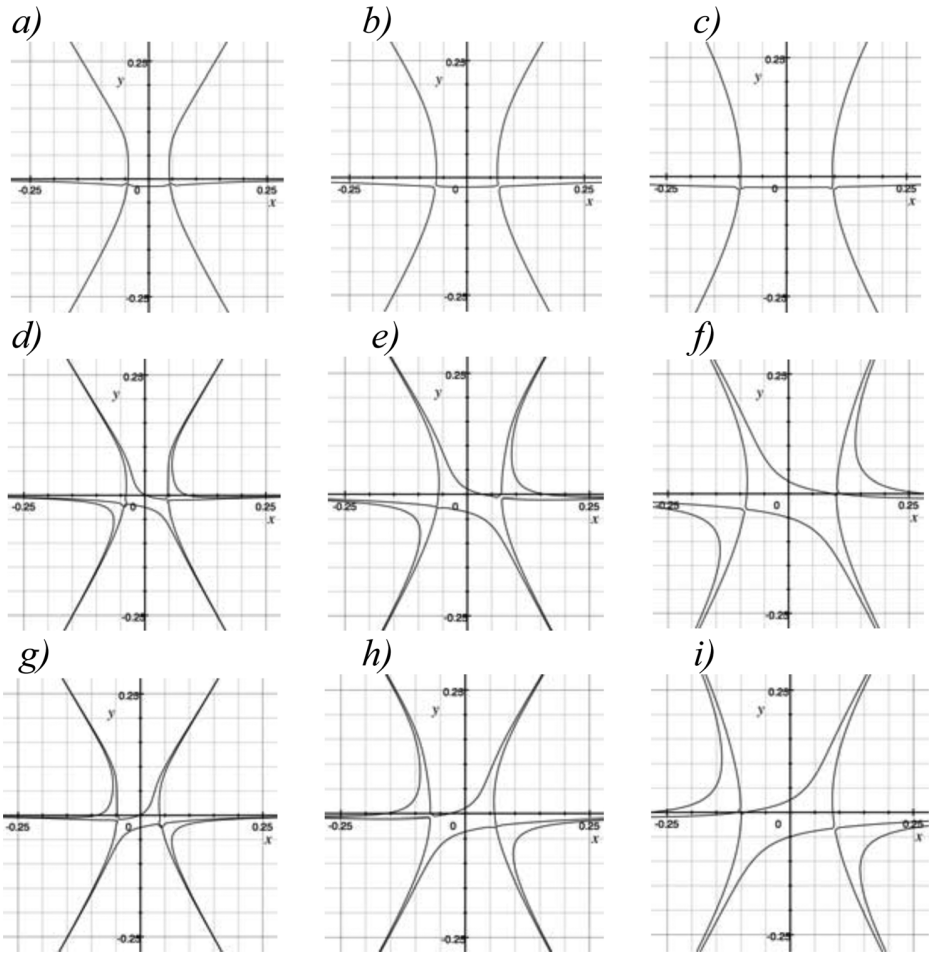

FIG. 25. Effect of the divertor current on the magnetic configuration of the snowflake divertor. In all cases, $j^{(0)}_{div}/\bar{j} = 0.1$. The parameter D_c/a is 0.05 in the left column, 0.1 in the central column, and 0.2 in the right column. In all panels, $d_{yc} = D_c$. In the first row, the current is distributed symmetrically with respect to the bisector $d_{xc} = 0$. In the second row, $d_{xc} = 0.5D_c$; in the last row, $d_{xc} = -0.5D_c$.

By adjusting the currents in PF coils, one can make $A_1 = 0$. Then, in the vicinity of the null, one can neglect the terms z^3 and higher in Eq. (D1) and z^4 and higher in Eq. (D2). We then find the snowflake field represented by Eq. (18).

By further adjustments of the currents, one can make both $A_1 = 0$ and $A_2 = 0$, thereby making the $A_3 z^3$ the first non-vanishing term in Eq. (D1). This situation corresponds to a cloverleaf divertor.[112]

We see that each step requires imposing additional constraints on the currents in PF coils. An example of a relatively simple coil arrangement for the cloverleaf divertor is described in Ref. 112. Moving further is, in principle, possible but looks at present unnecessary.

If on each step we do not completely remove the lower-order terms (due to, e.g., imperfect operation of the control system) but bring them to small values, we obtain configurations with several nearby nulls. Specifically, in the case (D4), we allow for a small linear contribution (A_1 small but finite) and we obtain a quasi-snowflake,with two nearby first-order nulls. Allowing for small but finite values for A_1 and A_2 in the cloverleaf case leads to a splitting of the third-order null to three first-order nulls.

[1]F. Najmabadi and the ARIES Team, "Overview of the ARIES-RS reversed-shear tokamak power plant study," Fusion Eng. Des. **38**, 3 (1997).
[2]S. Jardin, C. Kessel, T. Mau, R. Miller, F. Najmabadi, V. Chan, M. Chu, R. LaHaye, L. Lao, T. Petrie, P. Politzer, H. StJohn, P. Snyder, G. Staebler, A. Turnbull, and W. West, "Physics basis for the advanced tokamak fusion power plant, ARIES-AT," Fusion Eng. Des. **80**, 25 (2006).
[3]ITER Physics Expert Group on Divertor, ITER Physics Expert Group on Divertor Modelling, and Database, and ITER Physics Basis Editors, "Chapter 4: Power and particle control," Nucl. Fusion **39**, 2391 (1999).
[4]A. Loarte, B. Lipschultz, A. Kukushkin, G. Matthews, P. Stangeby, N. Asakura, G. Counsell, G. Federici, A. Kallenbach, K. Krieger, A. Mahdavi, V. Philipps, D. Reiter, J. Roth, J. Strachan, D. Whyte, R. Doerner, T. Eich, W. Fundamenski, A. Herrmann, M. Fenstermacher, P. Ghendrih, M. Groth, A. Kirschner, S. Konoshima, B. LaBombard, P. Lang, A. Leonard, P. Monier-Garbet, R. Neu, H. Pacher, B. Pegourie, R. Pitts, S. Takamura, J. Terry, E. Tsitrone, ITPA Scrape-off Layer, and D. P. T. Group, "Chapter 4: Power and particle control," Nucl. Fusion **47**, S203 (2007).
[5]M. Kotschenreuther, P. M. Valanju, S. M. Mahajan, and J. C. Wiley, "On heat loading, novel divertors, and fusion reactors," Phys. Plasmas **14**, 072502 (2007).
[6]L. Spitzer, "A proposed stellarator," AEC Report No. NYO-993, PM-S-1, 1951. In a subsequent talk of L. Spitzer's Princeton colleagues. C. R. Burnett, D. J. Grove, R. W. Palladino, T. H. Stix, and K. E. Wakefield, P/339, 1958 Geneva Conference, the following definition was introduced: "The divertor is a device, first proposed by L. Spitzer, for averting contact between the hot ionized gas and the wall of the main discharge tube." Note that in these first studies the authors meant to "divert" toroidal field, whereas the modern tokamak divertors are based on "diverting" the poloidal field. The latter allows for maintaining the toroidal symmetry of the tokamak magnetic system and avoiding enhanced particle losses associated with breaking of the toroidal symmetry. Note also that Spitzer's divertor was invented for the stellarators, where deviations form toroidal symmetry are in principle allowed. Conceptually, though, both toroidal and poloidal divertors introduce a separatrix and are in this regard very similar.
[7]F. Wagner, G. Becker, K. Behringer, D. Campbell, A. Eberhagen, W. Engelhardt, G. Fussmann, O. Gehre, J. Gernhardt, G. Vongierke, G. Haas,

M. Huang, F. Karger, M. Keilhacker, O. Kluber, M. Kornherr, K. Lackner, G. Lisitano, G. G. Lister, H. M. Mayer, D. Meisel, E. R. Muller, H. Murmann, H. Niedermeyer, W. Poschenrieder, H. Rapp, H. Rohr, F. Schneider, G. Siller, E. Speth, A. Stabler, K. H. Steuer, G. Venus, O. Vollmer, and Z. Yu, "Regime of improved confinement and high-beta in neutral-beam-heated divertor discharges of the asdex tokamak," Phys. Rev. Lett. **49**, 1408 (1982).
[8]F. Wagner, "A quarter-century of H-mode studies," Plasma Phys. Controlled Fusion **49**, B1–B33 (2007).
[9]M. Wischmeier, ASDEX Upgrade Team, and JET EFDA Contributors, "High density operation for reactor-relevant power exhaust," J. Nucl. Mater. **463**, 22–29 (2015).
[10]R. A. Pitts, S. Carpentier, F. Escourbiac, T. Hirai, V. Komarov, S. Lisgo, A. S. Kukushkin, A. Loarte, M. Merola, A. S. Baik, R. Mitteau, M. Sugihara, B. Bazylev, and P. C. Stangeby, "A full tungsten divertor for ITER: Physics issues and design status," J. Nucl. Mater. **438**, S48–S56 (2013).
[11]P. Stangeby, *The Plasma Boundary of Magnetic Fusion Devices* (Taylor & Francis, 2000).
[12]S. V. Mirnov, V. N. Dem'yanenko, and E. V. Muraviev, "Liquid-metal tokamak divertors," J. Nucl. Mater. **196–198**, 45 (1992).
[13]S. Mirnov, "Plasma-wall interactions and plasma behaviour in fusion devices with liquid lithium plasma facing components," J. Nucl. Mater. **390–391**, 876–875 (2009).
[14]M. L. Apicella, V. Lazarev, I. Lyublinski, G. Mazzitelli, S. Mirnov, and A. Vertkov, "Lithium capillary porous system behavior as PFM in FTU tokamak experiments," J. Nucl. Mater. **386–388**, 821–823 (2009).
[15]R. Majeski, T. Abrams, D. Boyle, E. Granstedt, J. Hare, C. M. Jacobson, R. Kaita, T. Kozub, B. LeBlanc, C. M. Jacobson, R. Kaita, D. P. Lundberg *et al.*, "Particle control and plasma performance in the lithium tokamak experiment," Phys. Plasmas **20**, 056103 (2013).
[16]A. Leonard, M. A. Mahdavi, S. L. Allen, N. H. Brooks, M. E. Fenstermacher, D. N. Hill, C. J. Lasnier, R. Maingi, G. D. Porter, T. W. Petrie, J. G. Watkins, and W. P. West, "Distributed divertor radiation through convection in DIII-D," Phys. Rev. Lett. **78**, 4769 (1997).
[17]A. Leonard, M. A. Mahdavi, C. J. Lasnier, T. W. Petrie, and P. C. Stangeby, "Scaling radiative divertor solutions to high power in DIII-D," Nucl. Fusion **52**, 063015 (2012).
[18]T. W. Petrie, M. R. Wade, N. H. Brooks, M. E. Fenstermacher *et al.*, "Compatibility of the radiating divertor with high performance plasmas on DIII-D," J. Nucl. Mater. **363–365**, 416 (2007).
[19]R. H. Cohen and D. D. Ryutov, "Plasma convection induced by toroidal asymmetries of the divertor plates and gas puffing," Nucl. Fusion **37**, 621 (1997).
[20]G. F. Counsell, J.-W. Ahn, R. H. Cohen, A. Kirk, P. Helander, R. Martin, D. D. Ryutov, A. Tabasso, H. R. Wilson, Y. Yang, and MAST Team, "Exhaust, ELM, and halo physics using the MAST tokamak," Nucl. Fusion **43**, 1197 (2003).
[21]S. J. Zweben, R. J. Maqueda, A. L. Roquemore, C. E. Bush, R. Kaita, R. J. Marsala, Y. Raitses, R. H. Cohen, and D. D. Ryutov, "Local scrape-off layer control using biased electrodes in NSTX," Plasma Phys. Controlled Fusion **51**, 105012 (2009).
[22]S. Potzel, M. Wischmeier, M. Bernert, R. Dux, H. W. Mueller, and A. Scaraboso, "A new experimental classification of divertor detachment in ASDEX upgrade," Nucl. Fusion **54**, 013001 (2014).
[23]B. Lipschultz, X. Bonnin, G. Counsell, A. Kallenbach, A. Kukushkin, K. Krieger, A. Leonard, A. Loarte, R. Neu, R. Pitts, T. Rognlien, J. Roth, C. Skinner, J. Terry, E. Tsitrone, D. Whyte, S. Zweben, N. Asakura, D. Coster, R. Doerner, R. Dux, G. Federici, M. Fenstermacher, W. Fundamenski, P. Ghendrih, A. Herrmann, J. Hu, S. Krasheninnikov, G. Kirnev, A. Kreter, V. Kurnaev, B. Labombard, S. Lisgo, T. Nakano, N. Ohno, H. Pacher, J. Paley, Y. Pan, G. Pautasso, V. Philipps, V. Rohde, D. Rudakov, P. Stangeby, S. Takamura, T. Tanabe, Y. Yang, and S. Zhu, "Plasma-surface interaction, scrape-off layer and divertor physics: implications for ITER," Nucl. Fusion **47**, 1189 (2007).
[24]R. C. J. Lasnier, D. N. Hill, T. W. Petrie, A. W. Leonard, T. E. Evans, and R. Maingi, "Survey of target plate heat fluxin diverted DIII-D tokamak discharges," Nucl. Fusion **38**, 1225 (1998).
[25]J. Kesner, "Triple X-point tokamak divertor," Nucl. Fusion **30**, 548 (1990).
[26]K. Bol, M. Okabayashi, and R. Fonck, "The poloidal divertor experiment (PDX) and the princeton beta experiment (PBX)," Nucl. Fusion **25**, 1149 (1985).
[27]H. Takase, "Guidance of divertor channel by cusp-like magnetic field for tokamak devices," J. Phys. Soc. Jpn. **70**, 609 (2001).
[28]M. Kotschenreuther, P. M. Valanju, J. Wiley, T. Rognlien, S. Mahajan, and M. Pekker, "Scrape off layer physics for burning plasmas and innovative divertor solutions," in *2004 IAEA Fusion Energy Conference, Vilamoura, Portugal, 1–6 November 2004* (International Atomic Energy Agency, Vienna, 2004), Paper No. IC/P6-43.
[29]M. Kotschenreuther, P. M. Valanju, S. M. Mahajan, J. C. Wiley, M. Pekker, W. L. Rowan, H. He, T. Rognlein, and D. Gates, "On heat loading, divertors and reactors," in *2006 IAEA Fusion Energy Conference, Chengdu, China, 16–21 October 2006* (International Atomic Energy Agency, Vienna, 2006), Paper No. IC/P7-12.
[30]R. A. Pitts, B. P. Duval, A. Loarte, J. M. Moret, J. A. Boedo, D. Coster, I. Furno, J. Horacek, A. S. Kukushkin, D. Reiter, and J. Rommers, "Divertor geometry effects on detachment in TCV," J. Nucl. Mater. **290**, 940 (2001).
[31]M. Kotschenreuther, P. M. Valanju, S. Mahajan, L. J. Zheng, L. D. Pearlstein, R. H. Bulmer, J. Canik, and R. Maingi, "The super x divertor (SXD) and high power density experiment (HPDX)," *2008 IAEA Fusion Energy Conference, Geneva, Switzerland, 13–18 October 2008* (International Atomic Energy Agency, Vienna, 2008), Paper No. IC/P4-7.
[32]I. Katramados, G. Fishpool, M. Fursdon, G. Whitfield, V. Thompson, and H. Meyer, "MAST upgrade closed pumped divertor design and analysis," Fusion Eng. Des. **86**, 1595 (2011).
[33]G. Fishpool, J. Canik, G. Cunningham, J. Harrison, I. Katramados, A. Kirk, M. Kovari, H. Meyer, R. Scannell, and MAST-Upgrade Team, "MAST-upgrade divertor facility and assessing performance of long-legged divertors," J. Nucl. Mater. **438**, S356 (2013).
[34]D. D. Ryutov, "Geometrical Properties of a "Snowflake" Divertor," Phys. Plasmas **14**, 064502 (2007).
[35]D. D. Ryutov, R. H. Cohen, T. D. Rognlien, and M. V. Umansky, "Magnetic field structure of a snowflake divertor," "Phys. Plasmas **15**, 092501 (2008).
[36]D. D. Ryutov, M. A. Makowski, and M. V. Umansky, "Local properties of the magnetic field in a snowflake divertor," Plasma Phys. Controlled Fusion **52**, 105001 (2010).
[37]Y. V. Gott, M. S. Ioffe, and V. G. Telkovsky, Nucl. Fusion **3**, 1045–1047 (1962).
[38]D. W. Kerst, H. K. Forsen, D. M. Meade, D. E. Lencioni, J. C. Sprott, H. V. de la Fuente, A. W. Molvik, R. A. Breun, A. J. Cavallo, J. R. Drake, J. R. Greenwood, T. C. Jernigan, R. Prater, and J. W. Rudmin, "Plasma injection, heating, confinement, and losses in multipole structures," in *Proceedings of the 4th IAEA Conference on Plasma Physics and Controlled Thermonuclear Fusion, 17–23 June 1971, Vienna* (1971), pp. 3–14.
[39]J. H. Halle, A. G. Kellman, R. S. Post, S. C. Prager, E. J. Strait, and M. C. Zarnstorff, "Observations of high-beta toroidal plasmas," Phys. Rev. Lett. **46**, 1394 (1981).
[40]M. S. Ioffe, B. I. Kanaev, V. V. Piterskii, and E. E. Yushmanov, "Plasma confinement in the Atoll electrostatically plugged magnetic cusp," Sov. J. Plasma Phys. **10**, 261 (1984).
[41]E. J. Synakowski, M. G. Bell, R. E. Bell, T. Bigelow *et al.*, "The national spherical torus experiment (NSTX) research programme and progress towards high beta, long pulse operating scenarios," Nucl. Fusion **43**, 1653 (2003).
[42]J. W. Brown and R. V. Churchill, *Complex Variables and Applications* (McGraw Hill, Boston/New York/Toronto, 2004).
[43]G. Haas, M. Keilhacker, W. Poschenrieder, H. Vernickel, and F. Wagner, "Aspects of plasma-wall interaction in the ASDEX divertor experiment," J. Nucl. Mater. **63**, 92 (1976).
[44]V. A. Soukhanovskii, R. E. Bell, A. Diallo, S. Gerhardt, S. Kaye, E. Kolemen, B. P. LeBlanc, A. McLean, J. E. Menard, S. F. Paul, M. Podesta, R. Raman, D. D. Ryutov, F. Scotti, R. Kaita, R. Maingi, D. M. Mueller, A. L. Roquemore, H. Reimerdes, G. P. Canal, B. Labit, W. Vijvers, S. Coda, B. P. Duval, T. Morgan, J. Zielinski, G. De Temmerman, and B. Tal, "Advanced divertor configurations with large flux expansion," J. Nucl. Mater. **438**, S96 (2013).
[45]S. Coda for the TCV Team, "Overview of recent and current research on the TCV tokamak," Nucl. Fusion **53**, 104011 (2013).
[46]S. A. Sabbagh and NSTX Team, "Overview of physics results from the conclusive operation of the National Spherical Torus Experiment," Nucl. Fusion **53**, 104007 (2013).
[47]D. N. Hill and DIII-D Team, "DIII-D research towards resolving key issues for ITER and steady-state tokamaks," Nucl. Fusion **53**, 104001 (2013). Details of the first snowflake experiments on DIII-D were

presented in a post-deadline talk by S. Allen *et al*., "Results from initial snowflake divertorphysics studies on DIII-D," paper presented at the PD/1-2 at the 2012 IAEA Conference, San Diego, CA.
[48]G. P. Canal *et al*., "Comparison between experiments and EMC-3-Eirene simulations of the snowflake divertor in TCV," BAPS **58**, 256 (2013).
[49]W. A. J. Vijvers, G. P. Canal, B. P. Duval, B. Labit, B. Lipschultz, T. Lunt, F. Nespoli, H. Reimerdes, U. Sheikh, C. Theiler, C. Tsui, K. H. A. Verhaegh, and TCV Team, "Advanced divertor research on the TCV tokamak," paper presented at the P2.150, EPS Plasma Conference, Lisbon, 2015.
[50]D. D. Ryutov, R. H. Cohen, T. D. Rognlien, and M. V. Umansky, "A snowflake divertor: Solving a power exhaust problem for tokamaks," Plasma Phys. Controlled Fusion **54**, 124050 (2012).
[51]M. V. Umansky, R. H. Bulmer, R. H. Cohen, T. D. Rognlien, and D. D. Ryutov, "Analysis of geometric variations in high-power tokamak divertors," Nucl. Fusion **49**, 075005 (2009).
[52]V. A. Soukhanovskii, R. E. Bell, A. Diallo, S. Gerhardt, S. M. Kaye, E. Kolemen, B. P. LeBlanc, A. McLean, J. E. Menard, S. F. Paul, M. Podesta, R. Raman, T. D. Rognlien, A. L. Roquemore, D. D. Ryutov, F. Scotti, M. Umansky, D. Battaglia, M. G. Bell, D. A. Gates, R. Kaita, R. Maingi, and S. A. Sabbagh, "Snowflake divertor configuration studies in NSTX," Phys. Plasmas **19**, 082504 (2012).
[53]T. D. Rognlien, R. H. Cohen, D. D. Ryutov, and M. V. Umansky, "Comparison of ELM heat loads in snowflake and standard divertors," J. Nucl. Mater. **438**, S418 (2013).
[54]V. Pericoli Ridolfini, R. Zagórski, G. Artaserse, G. Calabrò, F. Crisanti, G. Maddaluno, G. Ramogida, and B. Viola, "Preliminary 2D code simulation of the quasi-snowflake divertor configuration in the FAST tokamak," Fusion Eng. Des. **88**, 1677 (2013).
[55]E. T. Meier, V. A. Soukhanovskii, S. Gerhardt, J. E. Menard, and T. D. Rognlien, "Multi-fluid transport modeling of NSTX upgrade standard and snowflake divertor configurations," Contrib. Plasma Phys. **54**, 454 (2014).
[56]B. Viola, G. Corrigan, D. Harting, G. Maddaluno, M. Mattia, V. Pericoli Ridolfini, and R. Zagorski, "Preliminary comparison of the conventional and quasi-snowflake divertor configurations with the 2D code EDGE2D/EIRENE in the FAST tokamak," Contrib. Plasma Phys. **54**, 459 (2014).
[57]G. Pełka, R. Zagorski, V. P. Ridolfini, G. Artaserse, G. Calabro, F. Crisanti, G. Maddaluno, G. Ramogida, and B. Viola, "TECXY code simulation of snowflake divertor configuration in DEMO reactor," Contrib. Plasma Phys. **54**, 464 (2014).
[58]S. F. Mao, Y. Guo, X. B. Peng, Z. P. Luo, B. J. Xiao, Y. T. Song, D. M. Yao, S. Z. Zhu, and M. Y. Ye, "Evaluation of target-plate heat flux for a possible snowflake divertor in CFETR using SOLPS," J. Nucl. Mater. **463**, 1233 (2015).
[59]M. V. Umansky, T. D. Rognlien, D. D. Ryutov, and P. B. Snyder, "Edge plasma in snowflake divertor," Contrib. Plasma Phys. **50**, 350 (2010).
[60]Yu. Medvedev, A. A. Ivanov, A. A. Martynov, Yu. Yu. Poshekhonov, R. Behn, Y. R. Martin, J.-M. Moret, F. Piras, A. Pitzschke, A. Pochelon, O. Sauter, and L. Villard, "Edge stability and pedestal profile sensitivity of snowflake diverted equilibria in the TCV tokamak," Contrib. Plasma Phys. **50**, 324 (2010).
[61]J. F. Ma, X. Q. Xu, and B. D. Dudson, "Linear peeling–ballooning mode simulations in snowflake-like divertor configuration using BOUT++ code," Nucl. Fusion **54**, 033011 (2014).
[62]S. I. Krasheninnikov, "On scrape off layer plasma transport," Phys. Lett. A **283**, 368 (2001).
[63]D. Farina, R. Pozzoli, and D. D. Ryutov, "Effect of the magnetic field geometry on the flute-like perturbations near the divertor X-point," Nucl. Fusion **33**, 1315 (1993).
[64]B. Labit, A. Pochelon, M. Rancic, F. Piras, A. Bencze, A. Bottino, S. Brunner, Y. Camenen, P. K. Chattopadhyay, S. Coda, E. Fable, T. P. Goodman, S. Jolliet, A. Marinoni, L. Porte, B. F. McMillan, S. Yu. Medvedev, O. Sauter, V. S. Udintsev, L. Villard, and TCV Team, "Transport and turbulence with innovative plasma shapes in the TCV tokamak," in *2010 IAEA Fusion Energy Conference, Daejoen, Korea* (International Atomic Energy Agency, Vienna, 2010), Paper No. EXC/P8-08.
[65]B. Labit, I. Furno, H. Reimerdes, W. Vijvers, S. Coda, and TCV Team, "Scrape-off layer properties of single-null and snowflake diverted plasmas in TCV," in *EPS Plasma Conference, Strasbourg* (2011), Paper No. P2.076.
[66]D. D. Ryutov and M. V. Umansky, "Ion drifts in a snowflake divertor," Phys. Plasmas **17**, 014501 (2010).
[67]A. V. Chankin and G. M. McCracken, "Loss ion orbits at the tokamak edge," Nucl. Fusion **33**, 1459 (1993).
[68]C. S. Chang, S. Kue, and H. Weitzner, "X-transport: A baseline nonambipolar transport in a diverted tokamak plasma edge," Phys. Plasmas **9**, 3884 (2002).
[69]I. Joseph, "Driving toroidally asymmetric current through the tokamak scrape-off layer. II. Magnetic field structure and spectrum," Phys. Plasmas **16**, 052511 (2009).
[70]W. A. Farmer and D. D. Ryutov, "Axisymmetric curvature-driven instability in a model divertor geometry," Phys. Plasmas **20**, 092117 (2013); W. A. Farmer, "Ballooning modes localized near the null point of a divertor," Phys. Plasmas **21**, 042114 (2014).
[71]D. D. Ryutov, R. H. Cohen, W. A. Farmer, T. D. Rognlien, and M. V. Umansky, "The "churning mode" of plasma convection in the tokamak divertor region," Phys. Scr. **89**, 088002 (2014); D. D. Ryutov *et al*., "Corrigendum," Phys. Scr. **90**, 099501 (2015).
[72]R. Albanese, R. Ambrosino, and M. Mattei, "A procedure for the design of snowflake magnetic configurations in tokamaks," Plasma Phys. Controlled Fusion **56**, 035008 (2014).
[73]G. Y. Zheng, X. Q. Xu, D. D. Ryutov, Y. D. Pan, and T. Y. Xia, "Magnetic configuration flexibility of snowflake divertor for HL-2M," Fusion Eng. Des. **89**, 2621 (2014).
[74]B. LaBombard, E. Marmar, J. Irby, J. L. Terry, R. Vieira, G. Wallace, D. G. Whyte, S. Wolfe, S. Wukitch, S. Baek, W. Beck, P. Bonoli, D. Brunner, J. Doody, R. Ellis, D. Ernst, C. Fiore, J. P. Freidberg, T. Golfinopoulos, R. Granetz, M. Greenwald, Z. S. Hartwig, A. Hubbard, J. W. Hughes, I. H. Hutchinson, C. Kessel, M. Kotschenreuther, R. Leccacorvi, Y. Lin, B. Lipschultz, S. Mahajan, J. Minervini, R. Mumgaard, R. Nygren, R. Parker, F. Poli, M. Porkolab, M. L. Reinke, J. Rice, T. Rognlien, W. Rowan, S. Shiraiwa, D. Terry, C. Theiler, P. Titus, M. Umansky, P. Valanju, J. Walk, A. White, J. R. Wilson1, G. Wright, and S. J. Zweben, "ADX: A high field, high power density, advanced divertor and RF tokamak," Nucl. Fusion **55**, 053020 (2015).
[75]W. A. J. Vijvers, G. P. Canal, B. Labit, H. Reimerdes, B. Tal, S. Coda, G. De Temmerman, B. P. Duval, T. W. Morgan, J. J. Zielinski, and TCV Team, "Power exhaust in the snowflake divertor for L- and H-mode TCV tokamak plasmas," Nucl. Fusion **54**, 023009 (2014).
[76]V. A. Soukhanovskii, S. L. Allen, M. E. Fenstermacher, D. N. Hill, C. J. Lasnier, M. A. Makowski, A. G. McLean, W. H. Meyer, E. Kolemen, R. J. Groebner, A. W. Hyatt, A. W. Leonard, T. H. Osborne, and T. W. Petrie, "Radiative snowflake divertor studies in DIII-D," J. Nucl. Mater. **463**, 1191 (2015).
[77]F. Piras, S. Coda, I. Furno, J. M. Moret, R. A. Pitts, O. Sauter, B. Tal, G. Turri, A. Bencze, B. P. Duval, F. Felici, A. Pochelon, and C. Zucca, "Snowflake divertor plasmas on TCV," Plasma Phys. Controlled Fusion **51**, 055009 (2009).
[78]D. D. Ryutov, R. H. Cohen, T. D. Rognlien, V. A. Soukhanovskii, and M. V. Umansky, "Comment on "Magnetic geometry and physics of advanced divertors: The X-divertor and the snowflake" [Phys. Plasmas **20**, 102507 (2013)]," Phys. Plasmas **21**, 054701 (2014).
[79]V. A. Soukhanovskii, J.-W. Ahn, R. E. Bell, D. A. Gates, S. Gerhardt, R. Kaita, E. Kolemen, B. P. LeBlanc, R. Maingi, M. Makowski, R. Maqueda, A. G. McLean, J. E. Menard, D. Mueller, S. F. Paul, R. Raman, A. L. Roquemore, D. D. Ryutov, S. A. Sabbagh, and H. A. Scott, "Taming the plasma-material interface with the 'snowflake' divertor in NSTX," Nucl. Fusion **51**, 012001 (2011).
[80]G. Calabrò, G. Artaserse, F. Crisanti, G. Ramogida, G. Maddaluno, P. Micozzi, V. Pericoli-Ridolfini, and B. Viola, "Snowflake divertor plasma studies on FAST proposal," in *38th EPS Conference on Plasma Physics* (2011), Paper No. P1.066.
[81]G. Calabrò, S. L. Chen, Y. Guo, J. G. Li, W. Liang, Z. P. Luo, B. J. Xiao, J. Xu, R. Albanese, R. Ambrosino, L. Barbato, F. Crisanti, E. Giovannozzi, S. Mastrostefano, A. Pironti, V. Pericoli Ridolfini, G. Ramogida, A. A. Tuccillo, F. Villone, B. Viola, R. Zagórski and EAST Team, "EAST snowflake experiment: Scenario development and edge simulations," in *2014 IAEA Fusion Energy Conference, St. Petersberg, Russia, 16–21 October* (International Atomic Energy Agency, Vienna, 2014), Paper No. EX/P3-4.
[82]Y. Gribov, D. Humphreys, K. Kajiwara, E. A. Lazarus, J. B. Lister, T. Ozeki, A. Portone, M. Shimada, A. C. C. Sips, and J. C. Wesley, "Chapter 8: Plasma operation and control," Nucl. Fusion **47**, S385–S403 (2007).

[83]R. Ambrosino, R. Albanese, S. Coda, M. Mattei, J.-M. Moret, and H. Reimerdes, "Optimization of experimental snowflake configurations on TCV," Nucl. Fusion **54**, 123008 (2014).
[84]E. Kolemen, S. L. Allen, B. D. Bray, M. E. Fenstermacher, D. A. Humphreys, A. W. Hyatt, C. J. Lasnier, A. W. Leonard, M. A. Makowski, A. G. McLean, R. Maingi, R. Nazikian, T. W. Petrie, V. A. Soukhanovskii, and E. A. Unterberg, "Heat flux management via advanced magnetic divertor configurations and divertor detachment," J. Nucl. Mater. **463**, 1186–1190 (2015).
[85]M. A. Makowski and D. Ryutov, "X-point tracking algorithm for the snowflake divertor," LLNL Report, 2009 (unpublished).
[86]T. Lunt, G. P. Canal, B. P. Duval, Y. Feng, B. Labit, P. McCarthy, H. Reimerdes, W. A. J. Vijvers, M. Wischmeier and EUROfusion MST1 Team, "Optimization of the snowflake divertor by means of EMC3-Eirene simulations and experiments," *42nd EPS Conference on Plasma Physics, Lisbon* (2015), Paper No. O4.115.
[87]T. D. Rognlien, J. L. Milovich, M. E. Rensink, and G. D. Porter, "A fully implicit, time-dependent 2-d fluid code for modeling tokamak edge plasmas," J. Nucl. Mater. **196**, 347 (1992).
[88]T. D. Rognlien and M. E. Rensink, "Edge-plasma models and characteristics for magnetic fusion energy devices," Fusion Eng. Des. **60**, 497 (2002).
[89]R. Schneider, X. Bonnin, K. Borrass, D. P. Coster, H. Kastelewicz, A. Reiter, V. A. Rozhansky, and B. J. Braams, "Plasma edge physics with B2-Eirene," Contrib. Plasma Phys. **46**, 3–191 (2006).
[90]T. Lunt, G. P. Canal, Y. Feng, H. Reimerdes, B. P. Duval, B. Labit, W. A. J. Vijvers, D. P. Coster, K. Lackner, and M. Wischmeier, "First edge Monte Carlo 3D-eirene simulations of the TCV snowflake divertor," Plasma Phys. Controlled Fusion **56**, 035009 (2014).
[91]H. Reimerdes, G. P. Canal, B. P. Duval, B. Labit, T. Lunt, W. A. J. Vijvers, S. Coda, G. De Temmerman, T. W. Morgan, F. Nespoli, B. Taland, and TCV Team, "Power distribution in the snowflake divertor in TCV," Plasma Phys. Controlled Fusion **55**, 124027 (2013).
[92]R. H. Cohen and D. D. Ryutov, "Electric drift, plasma current and Bohm condition in the SOL of a tokamak with a toroidal limiter," Comments Plasma Phys. Controlled Fusion **16**, 255 (1995).
[93]T. D. Rognlien, N. Mattor, G. D. Porter, and D. D. Ryutov, "2-D electric fields and drifts near the magnetic separatrix in divertor tokamaks," Phys. Plasmas **6**, 1851 (1999).
[94]M. J. Schaffer, J. A. Boedo, R. A. Moyer, T. N. Carlstrom, and J. G. Watkins, "Large EXB convection near the divertor X-point," JNM **290–293**, 530 (2001).
[95]S. S. Abdullaev, M. Jakubowski, M. Lehnen, O. Schmitz, and B. Unterberg, "On description of magnetic stochasticity in poloidal divertor tokamaks," Phys. Plasmas **15**, 042508 (2008).
[96]A. B. Rechester and M. N. Rosenbluth, "Electron heat-transport in a tokamak with destroyed magnetic surfaces," Phys. Rev. Lett. **40**, 38 (1978).
[97]T. E. Evans, "ELM mitigation techniques," J. Nucl. Mater. **438**, S11 (2013).
[98]G. Z. Gershuni and E. M. Zhukhovitski, "Convective stability of incompressible fluids," in Israel Program for Scientific Translations, Jerusalem, 1976.
[99]D. D. Ryutov, R. H. Cohen, E. Kolemen, L. LoDestro, M. Makowski, J. Menard, T. D. Rognlien, V. A. Soukhanovskii, M. V. Umansky, and X. Xu, "Theory and simulations of ELM control with a snowflake divertor," *2012 IAEA Fusion Energy Conference, San Diego, 16–21 October 2012* (International Atomic Energy Agency, Vienna, 2012), Paper No. TH/P4-18.
[100]R. J. Goldston, "Heuristic drift-based model of the power scrape-off width in low-gas-puff H-mode tokamaks," Nucl. Fusion **52**, 013009 (2012).
[101]F. Piras, S. Coda, B. P. Duval, B. Labit, J. Marki, S. Y. Medvedev, J.-M. Moret, A. Pitzschke, O. Sauter, and TCV Team, ""Snowflake" H mode in a tokamak plasma," Phys. Rev. Lett. **105**, 155003 (2010).
[102]F. Piras, S. Coda, B. P. Duval, B. Labit, J. Marki, S. Yu. Medvedev, J.-M. Moret, A. Pitzschke, O. Sauter, and TCV Team, "Snowflake divertor experiments on TCV," Plasma Phys. Controlled Fusion **52**, 124010 (2010).
[103]T. W. Petrie, S. L. Allen, M. E. Fenstermacher, R. J. Groebner, C. T. Holcomb, E. Kolemen, R. J. La Haye, C. J. Lasnier, A. W. Leonard, T. C. Luce, A. G. McLean, R. Maingi, R. A. Moyer, W. M. Solomon, V. A. Soukhanovskii, F. Turco, and J. G. Watkins, "Application of the radiating divertor approach to innovative tokamak divertor concepts," J. Nucl. Mater. **463**, 1225 (2015).
[104]H. Reimerdes, G. P. Canal, B. P. Duval, B. Labit, T. Lunt *et al.*, "Experimental investigation of neon seeding in the snowflake configuration TCV," J. Nucl. Mater. **463**, 1196 (2015).
[105]Z. Luo, B. Xiao, Y. Guo, and M. Ye, "Concept design of optimized snowflake diverted equilibria in CFETR," IEEE Trans. Plasma Sci. **42**, 1021 (2014).
[106]K. Lackner and H. Zohm, "Calculation of realistic snowflake equilibria for next-step devices," Fusion Sci. Technol. **63**, 43 (2013).
[107]N. Asakura, K. Hoshino, K. Shimizu, K. Shinya, H. Utoh, S. Tokunaga, K. Tobita, and N. Ohno, J. Nucl. Mater. **463**, 1238 (2015).
[108]X. Peng, M. Ye, Y. Song, X. Mao, P. Chen, and X. Qian, "Engineering conceptual design of CFETR divertor," Fusion Eng. Des. **98–99B** 1380–1383 (2015).
[109]D. D. Ryutov, S. I. Krasheninnikov, and T. D. Rognlien, "Model of convective, fully detached snowflake divertor," BAPS **58**, 253 (2013).
[110]M. Kotschenreuther, P. Valanju, B. Covelle, and S. Mahajan, "Magnetic geometry and physics of advanced divertors: The X-divertor and the snowflake," Phys. Plasmas **20**, 102507 (2013).
[111]D. D. Ryutov, "A "snowflake" divertor and its properties," in *2007 EPS Conference on Plasma Physics, Warsaw, Poland* (2007), Paper No. D1.002.
[112]D. D. Ryutov and M. V. Umansky, "Divertor with a third-order null of the poloidal field," Phys. Plasmas **20**, 092509 (2013).